Cascading flood-landslide scenarios reframe the hazard assessment of exposed infrastructure

International Journal of Disaster Risk Reduction 143 (2026) 106284

Contents lists available at ScienceDirect

International Journal of Disaster Risk Reduction

journal homepage: www.elsevier.com/locate/ijdrr

Cascading flood-landslide scenarios reframe the hazard assessment of exposed infrastructure

Margherita Lombardo [a], Giulia Evangelista [b], Pierluigi Claps [b], Pierfranco Costabile [a,*]

[a] University of Calabria, Department of Environmental Engineering, via P. Bucci, Rende, CS, 87036, Italy
[b] Department of Environment, Land and Infrastructure Engineering, Politecnico di Torino, Corso Duca degli Abruzzi 2, Turin, 10129, Italy

ABSTRACT

Conventional multi-hazard assessments in catchment-infrastructure configurations based on spatial overlay do not always capture physically interacting hazard chains, because they lack systematic protocols for identifying possible cascading activation. This structural limitation means that secondary impact pathways, possibly determined by geomorphological and hydraulic conditions, can remain undetected until damage occurs. This study addresses this gap by proposing a hierarchical stepwise framework that links regional screening with targeted field inspections and two-dimensional rain-on-grid hydrodynamic modelling to identify cascading geo-hydrological impact pathways threatening wastewater treatment plants (WWTPs) in small steep ungauged coastal catchments. Applied to 26 catchments along the Tyrrhenian coast of Calabria Region (southern Italy), the selection procedure identifies and classifies sites according to their predisposition to cascading hazard activation. Among these cases, the Maddalena catchment, a site exhibiting multi-pathway cascading potential based on field inspections, is selected as demonstrator for a full process-based modelling. Results show that landslide-induced channel obstruction generates backwater effects that reduce considerably the flood return period required to inundate the most vulnerable WWTP components. The reduction increases the frequency of a 1-in-500 year event under clear-water conditions to approximately a 1-in-50 year event under cascading conditions. Sensitivity analyses confirm that this threshold shift persists across different sediment distribution configurations and for landslide volume reductions up to 40%, demonstrating the robustness of the cascading mechanism. These findings show that multi-hazard overlay approaches can substantially underestimate latent flood-related environmental hazards in data-scarce environments, and that systematic cascading hazard screening provides actionable information for prioritising monitoring and protection of critical infrastructure in flood-prone coastal regions.

1. Introduction

Small steep coastal catchments in Mediterranean environments are characterised by short hydrological response times, confined valley geometries, and direct hillslope-to-coast connectivity that produce rapidly evolving flood dynamics with limited attenuation capacity. In these systems, geomorphological perturbations, such as landslide-induced sediment production, can substantially modify hydraulic conveyance and trigger non-linear changes in flood characteristics that extend well beyond the directly affected reach. These physically interacting hazard chains represent a structural challenge for conventional risk assessment. Using conventional multi-hazard approaches based on spatial overlay one overlaps single-hazard maps (e.g., flood and landslide hazard maps) whereby each process is evaluated independently. When considering critical infrastructure located in terminal reaches, this decoupled assessment also implies a temporal decoupling, leading to differentiated approaches for risk reduction. As a matter of fact, natural hazards are not always independent. For instance, flooding and landslides often exhibit significant temporal correlation (e.g. Ref. [1]), as both are

* Corresponding author.
E-mail addresses: margherita.lombardo@unical.it (M. Lombardo), giulia.evangelista@polito.it (G. Evangelista), pierluigi.claps@polito.it (P. Claps), pierfranco.costabile@unical.it (P. Costabile).

https://doi.org/10.1016/j.ijdrr.2026.106284
Received 17 May 2026; Received in revised form 25 June 2026; Accepted 27 June 2026
Available online 30 June 2026

driven by extreme rainfall events. In principle, spatial overlay approaches may still be applicable in cases where the spatial correlation between flooding and landslides is negligible, i.e., when they occur in non-connected areas. However, such approaches are unable to capture the amplification mechanisms that arise when one hazard alters the system state experienced by another. This occurs when the domain of influence of landslides interacts with that of flooding, for example when mobilised material encroaches upon inundated areas.

The conceptual distinction between multiple hazards, i.e. independent events assessed jointly without implying causal relationships ([2]), and cascading hazards, i.e. sequential processes in which one event modifies system state and propagates effects through explicit cause–effect chains, is well established in the literature ([3–5]), and explicitly recognised within European disaster risk reduction and integrated risk management policies ([6,7]). This distinction has direct methodological implications. Standard multi-hazard assessment frameworks, whether stochastic ([8,9]) or indicator-based ([10–14]), evaluate hazards independently and combine them through spatial overlay or regression techniques. Even approaches that incorporate interaction terms or dependency structures ([15,16]) stop short of explicitly resolving physical cause–effect chains. As a result, hazard amplification mechanisms that emerge only when one process modifies the hydraulic or geomorphological state of the system, as occurs when landslide deposits obstruct a channel and generate backwater effects upstream, remain systematically outside the scope of conventional assessments.

Cascading hazard chains involving geomorphological and hydrological processes are well documented in the literature ([17]). Intense or prolonged rainfall can exceed the infiltration capacity of steep unconsolidated slopes, triggering landslides and debris flows that deliver large volumes of sediment to the channel network ([18,19]). Once deposited, this material reduces cross-sectional conveyance capacity, generating backwater effects and substantially amplifying flood hazard in upstream reaches ([20]). Antecedent landscape disturbances, such as wildfires, can further precondition catchments to this type of response by altering infiltration

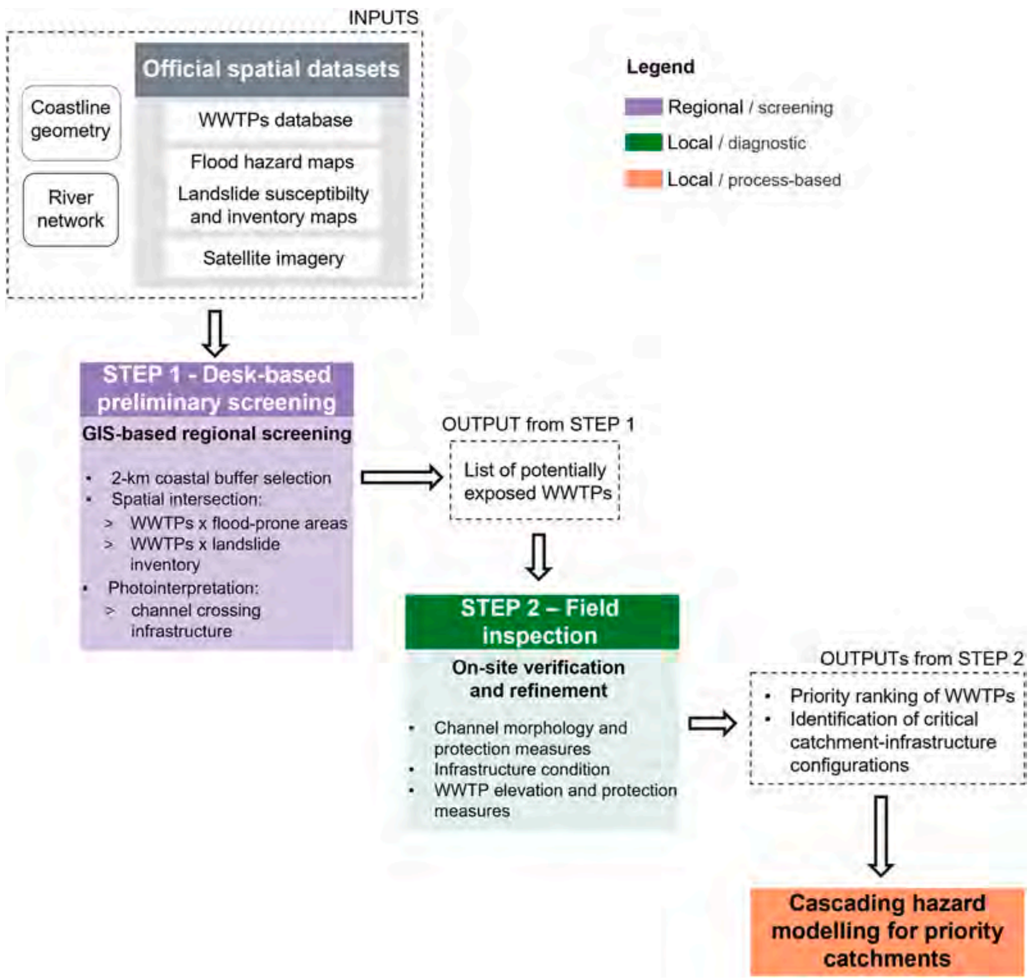

Fig. 1. Hierarchical stepwise framework for catchment–infrastructure screening and selection. The framework progressively increases spatial resolution and analytical detail, enabling the identification and prioritisation of wastewater treatment plants (WWTPs) susceptible to flood- and landslide-driven cascading impact pathways.

capacity and increasing sediment availability ([21,22]). In small coastal mediterranean catchments, where channel gradients are steep and response times are short, even moderate geomorphological perturbations can disproportionately alter flood dynamics, creating conditions for hazard amplification that static multi-hazard assessments are structurally unable to detect.

Despite this growing body of literature, most cascading hazard studies focus on detailed process-based modelling of individual catchments, typically selected a posteriori on the basis of observed damage or known criticalities ([4]). While such analyses provide valuable mechanistic insight, they do not address the prior question of how to systematically identify, at regional scale, which catchment–infrastructure configurations are structurally predisposed to cascading hazard activation. This absence of a systematic identification step means that potentially critical sites, where geomorphological and hydraulic conditions create latent cascading pathways, remain undetected until an event reveals them. The transferability of existing findings is consequently limited, and the gap between site-specific process understanding and regional risk screening remains largely unaddressed.

This study addresses both gaps by proposing a hierarchical stepwise framework that systematically links regional desk-based screening with targeted field inspections and detailed two-dimensional rain-on-grid hydrodynamic modelling to identify cascading geo-hydrological impact pathways threatening infrastructure in small steep ungauged coastal catchments.

Among infrastructure that interfere with rivers, wastewater treatment plants (WWTPs) are particularly exposed under flooding conditions, as they are commonly located in low-lying coastal areas to serve populations living close to the coast. They are often sited directly in the path of small watercourses, where floodwaters often convey substantial sediment and debris content. The environmental and sanitary consequences of WWTP flooding are well documented ([23–25]), and neglecting flood-driven infrastructure failure can lead to systematic underestimation of the societal and ecological costs of extreme events ([26–28]).

Unlike previous studies that apply cascading hazard modelling to pre-selected sites, the framework introduced here formalises the identification step as a reproducible, criteria-based procedure applicable to data-scarce environments, enabling systematic prioritisation of sites predisposed to cascading hazard activation before detailed modelling is undertaken. The framework is applied to 26 catchments along the Tyrrhenian coast of Calabria (southern Italy); the Maddalena catchment, identified as representative of multi-pathway cascading sites through field inspections, serves as a demonstrator for full process-based modelling. While applied to a specific Mediterranean coastal area, the framework is designed to be transferable to comparable ungauged environments characterised by steep topography and infrastructure encroachment along confined channels. The paper is organized as follows: Section 2 presents the hierarchical framework and cascading hazard modelling methodology; Section 3 describes the study area; Section 4 reports the results of screening and modelling; Section 5 discusses the implications for multi-hazard assessment and infrastructure risk management; Section 6 draws conclusions.

2. Hierarchical stepwise framework and cascading hazard modelling

The proposed framework operates through three progressive steps of increasing spatial resolution and computational demand, designed to concentrate analytical effort on sites where cascading hazard activation is most plausible. Step 1 consists of a GIS-based desk screening of regional catchment–infrastructure configurations using publicly available hazard and infrastructure datasets. Step 2 applies targeted field inspections to verify and classify sites retained after screening according to their dominant cascading mechanism. Step 3 implements detailed two-dimensional rain-on-grid hydrodynamic modelling on priority catchments, incorporating digital terrain modifications to represent landslide-induced channel obstruction. The catchment screening and classification procedure is described in Section 2.1 and illustrated in Fig. 1; the cascading hazard modelling framework is presented in Section 2.2.

2.1. Hierarchical framework for catchment-infrastructure screening and prioritisation

2.1.1. STEP 1: desk-based preliminary screening

The first step consists of a GIS-based preliminary screening to identify priority sites for a cascading hazard analysis based on large scale official information. This phase utilises publicly available spatial datasets to assess the exposure of coastal wastewater treatment plants (WWTPs) to flood and landslide hazards.

The screening integrates the following information:

- WWTPs database: georeferenced locations of wastewater treatment facilities, including plant identifiers, treatment capacity (population equivalents), and managing entities;
- flood hazard maps: ISPRA (Italian Institute for Environmental Protection and Research), delineating flood-prone areas according to the EU Floods Directive (2007/60/EC) return period scenarios (high, medium, and low probability);

Table 1
Rationale, screening criteria, and GIS-based methods used to identify and assess coastal WWTPs.

Rationale	Criterion	Method
Coastal proximity	WWTP within 2 km coastline	Buffering
Hydraulic exposure	Intersection with flood hazard	Layer intersection
Landslide exposure	Proximity to landslide hazard	Layer intersection
Amplification factor	Transport network intersection	Photointerpretation

- landslide hazard maps: ISPRA landslide susceptibility and inventory maps (IdroGEO platform, data available at: idrogeo.isprambiente.it/app/pir, last access: 03/02/2026);
- satellite imagery: Google Satellite basemap for visual verification and photointerpretation.

A 2-km coastal buffer was applied to select relevant facilities, which were then intersected with flood-prone areas and landslide inventories to identify sites partially or fully exposed to hydraulic hazard and landslide hazard. The presence of channel-crossing infrastructure, bridges or road crossings, was assessed through systematic satellite image photointerpretation. Screening criteria and their rationale are summarised in Table 1.

Step 1 is deliberately conservative: screening criteria are designed to retain all sites where cascading hazard activation cannot be excluded on the basis of regional data alone, accepting a proportion of false positives in order to minimise the risk of discarding genuinely critical configurations before field verification.

2.1.2. STEP 2: inspection objectives and protocol

Desk-based screening represents a necessary preliminary step, although it is inherently constrained by the use of regional datasets that may not fully capture the site-specific conditions governing cascading hazard activation. Regional flood hazard maps are typically based on morphology-driven criteria that may not reflect actual channel conveyance capacity. Similarly, landslide inventories document historical instabilities but do not necessarily provide detailed information on current slope conditions, sediment availability, or the spatial relationship between unstable areas and the active channel. Field inspections are therefore applied as a second-level verification step to observe directly channel morphology, hydraulic structure condition, WWTP layout, and functional connectivity between hillslopes, waterways, and exposed infrastructure, the site-specific factors that determine whether a cascading pathway is physically plausible. The aim of this step is not to provide a deterministic hazard classification, but to reduce the modelling domain to configurations where cascading amplification is physically reasonable.

Based on field-observable indicators, retained sites are classified into three categories according to their dominant channel–infrastructure interaction mechanism, summarised in Table 2.

Category C1 encompasses sites where WWTP exposure arises primarily from backwater effects generated by bridge piers or abutments constricting the active channel. Category C2 includes proximity-driven configurations, where limited separation between the WWTP and a channelised or culverted reach, in the absence of protective measures, results in direct exposure to overflow or bank erosion during flood events. Category C3 identifies sites with multi-pathway cascading potential, characterised by the combined presence of active or relict slope instability and hydraulic connectivity with the channel, enabling hillslope–channel interaction mechanisms that couple geomorphological modification with flood dynamics.

Sites in categories C1 and C2 are exposed primarily through hydraulic processes and should be assessed through standard hydraulic modelling approaches, which are adequate to capture the dominant exposure mechanisms identified in Table 2. C3 sites are additionally predisposed to hazard amplification through landslide-induced modification of channel morphology and conveyance capacity, generating flood scenarios that cannot be captured by clear-water hydraulic modelling alone and that require the cascading framework developed in Section 2.2. Sites for which field evidence indicates negligible hazard–facility interaction are excluded from further analysis. Although the classification does not rely on fixed numerical thresholds, it is supported by observable indicators, including channel freeboard relative to critical WWTP elevations, valley narrowing or local confinement, proximity between mapped landslide source areas and the active channel, and limited infrastructure setback from the channel margin. These elements can be identified using standard geomorphological survey methods.

2.2. Cascading hazard modelling for priority catchments

In this study, cascading interaction is conceptualised not as a strictly time-sequential chain of triggered hazards, but as a state-dependent mechanism in which pre-existing geomorphological alterations, specifically landslide-induced channel obstruction, modify the hydraulic response of the system and amplify the impact of subsequent hydrometeorological forcing. This framing explicitly captures a class of hazard interactions that static multi-hazard overlays cannot represent, as the amplification mechanism emerges only through an intermediate modification of system state that is invisible to independent hazard assessments.

Two hazard scenarios are defined on this basis. Scenario A considers intense rainfall under saturated antecedent soil conditions as the sole forcing, producing riverine flooding without geomorphological modification of the channel (cascade 1, Fig. 2). Scenarios B and

Table 2
Classification of sites by dominant cascading mechanism.

Category	Dominant Mechanism	Key field indicators	Cascading predisposition
C1	Backwater from channel-crossing infrastructure	Bridge piers, abutments within active channel, limited freeboard	Hydraulic constriction amplifies flood stage upstream of WWTP
C2	Proximity-driven direct exposure	WWTP adjacency to channelised or culverted reach, absence of protective barriers	Overflow, bank erosion, or structural failure during flood events
C3	Multi-pathway hillslope–channel interaction	Active or relict landslides on channel banks, hydraulic continuity with WWTP	Geomorphological modification of channel coupled with flood dynamics

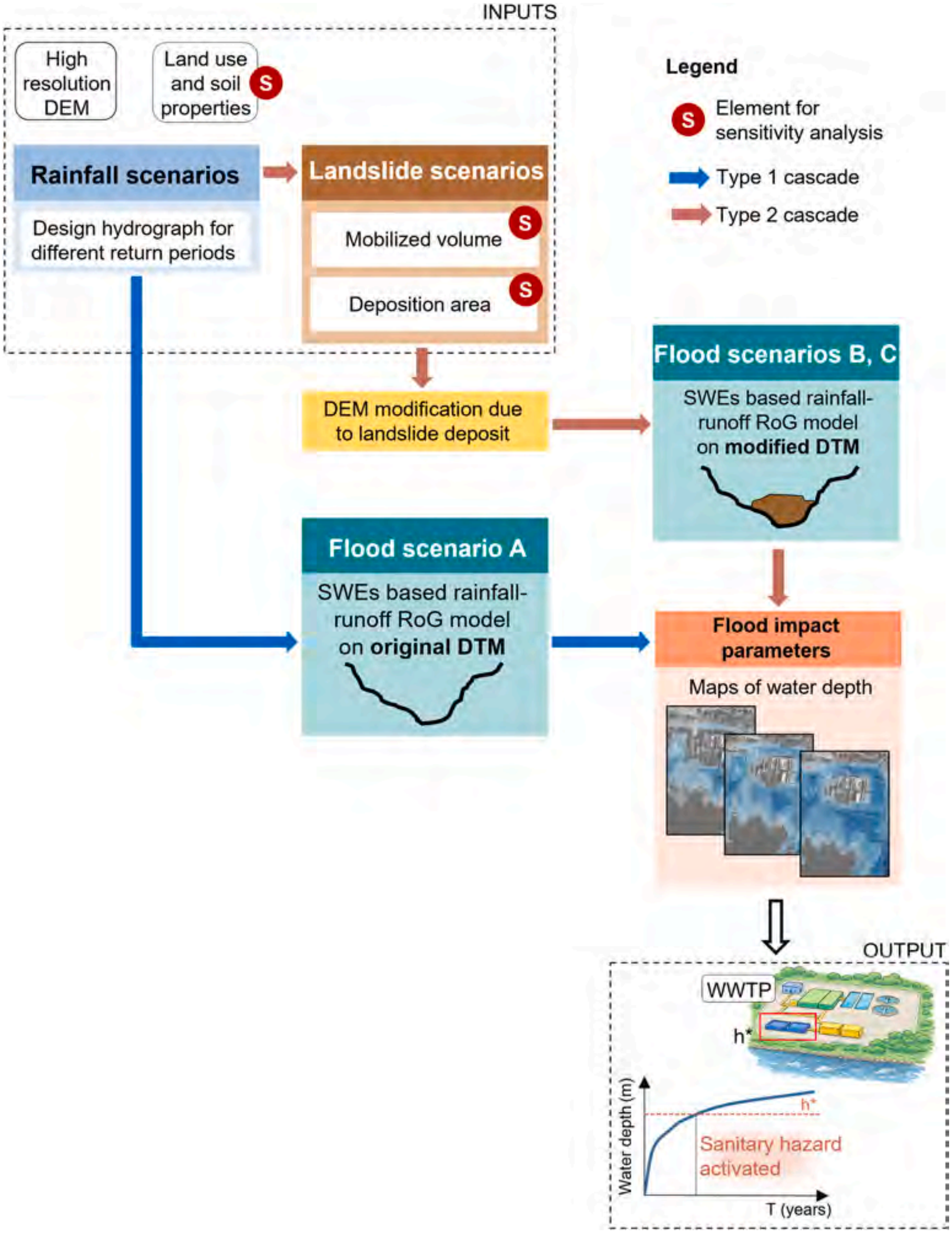

Fig. 2. Conceptual scheme of the cascading-hazard framework applied in this study. Design rainfall scenarios drive two-dimensional rain-on-grid flood simulations on the original digital elevation model (DTM) (flood scenario A) and on a modified DTM accounting for pre-existing landslide deposits (flood scenarios B and C). Landslide scenarios are defined in terms of mobilised volume and deposition area. Simulated water depths are then used to quantify flood impacts and to determine the minimum rainfall return period that triggers sanitary hazard activation, based on a threshold defined at the sludge treatment unit and adopted as a proxy for sanitary hazard. Red circles indicate elements explored through sensitivity analysis.

C introduce pre-existing landslide deposits within the channel at the onset of the flood event, representing two alternative sediment distribution patterns, i.e. uniform aggradation and channel-concentrated deposition respectively, that obstruct flow, induce backwater effects, and substantially increase upstream inundation extent (cascade 2, Fig. 2). The specific cascading configuration modelled here is grounded in field evidence collected during site inspections, as described in Section 2.1.2. Landslide source areas, mobilisable volumes, and deposition extents were estimated from the Italian Landslide Inventory (IFFI) and regional susceptibility maps available through the IdroGEO platform, as detailed in Appendix A1.

Landslide-induced channel obstruction is represented through local modification of the digital terrain model within the reach identified during field inspections as most susceptible to sediment deposition. Two deposition configurations are considered to bracket the range of plausible sediment redistribution patterns. Configuration B assumes uniform aggradation across the channel cross-section, representing a scenario in which deposited material spreads laterally across the full channel width (Fig. 3a). Configuration C assumes preferential accumulation in the thalweg, generating a spatially heterogeneous increase in bed elevation that concentrates obstruction in the deepest portion of the cross-section (Fig. 3b). In both configurations, the total volume delivered to the channel is identical; the two scenarios differ exclusively in the spatial redistribution of that volume across the cross-section. Moreover, in both cases, deposit thickness is derived from the local stage–volume relationship and the effective depositional surface available within the channel, as detailed in Appendix A1.

These two configurations represent physically plausible end-members of sediment distribution following a landslide delivery event, and their combined use provides a basis for assessing the sensitivity of the cascading hazard outcome to deposition geometry. The assumption of complete in-channel deposition represents a conservative upper-bound configuration: concentrating the full landslide volume within the channel cross-section maximises obstruction height and minimises residual conveyance capacity for a given mobilised volume, thereby producing the largest physically plausible backwater effect. Partial deposition, by distributing material across a wider area, would reduce unit obstruction height and attenuate backwater magnitude proportionally. This upper-bound assumption is therefore justified on geometric and hydraulic grounds prior to any modelling result, and its sensitivity is further explored through the volume-reduction analysis in Section 4.2.

Impact assessment focuses on the WWTP located within the study catchment. The most hydraulically exposed facility components are identified on the basis of their ground elevation relative to the surrounding terrain, as described in Section 4. The application of specific damage functions goes beyond the purpose of the work. Instead, exceedance of the corresponding elevation threshold by simulated water depths is used as a conservative operational proxy for the onset of conditions under which sludge mobilisation and environmental contamination may occur, consistent with the approach of using facility component elevation as a flood exposure threshold in WWTP vulnerability assessments ([23,25]). Specifically, the modelling framework identifies the hydraulic threshold conditions under which cascading amplification becomes physically possible, assuming the presence of a morphologically pre-conditioned channel state. The analysis identifies, for each scenario, the minimum rainfall return period required to exceed the defined threshold and is explicitly structured on a scenario-based approach. The occurrence probability of the pre-existing landslide condition is not explicitly estimated, nor is the joint probability of landslide activation and extreme rainfall formally quantified, as this lies beyond the scope of the present study.

The modelling framework comprises four components, detailed in the following sections: design rainfall scenario definition (Section 2.2.1), landslide volume estimation (Section 2.2.2, Appendix A1), two-dimensional hydrodynamic model setup and simulation (Section 2.2.3, Appendix A2), and sensitivity analysis on key sources of uncertainty including landslide volume, sediment distribution, surface roughness, and runoff generation method (Appendix A3).

For small ungauged catchments, where the absence of streamflow records precludes the direct application of statistical flood frequency methods, a rainfall-based approach is adopted: design hyetographs derived from IDF curves are used as input to a rain-on-grid hydrodynamic model, which directly simulates the flood hydrograph at the reach of interest without requiring a separate flood frequency analysis. Peak discharge was also estimated using the Rational Method as an independent order-of-magnitude check, given its widespread use for small ungauged catchments. The comparison between the two flood peaks is reported in Appendix A3.

The rainfall scenarios defined in Section 2.2.1 serve as direct input to the rain-on-grid model described in Section 2.2.2.

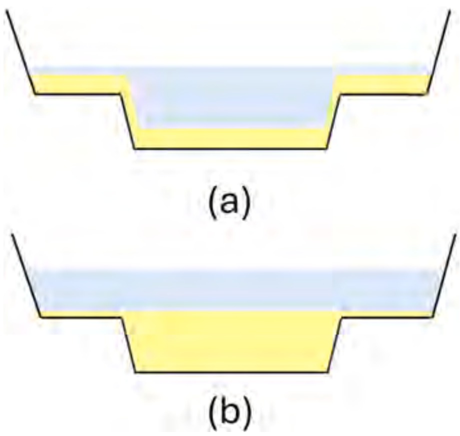

Fig. 3. Schematic representation of landslide-derived sediment distribution within the channel cross-section for the two deposition configurations considered: (a) uniform aggradation across the full channel width (flood scenario B) and (b) channel-concentrated deposition in the thalweg (flood scenario C). Both configurations assume complete delivery of the estimated landslide volume to the channel reach. The deposit volume within the cross section is shown in yellow. (For interpretation of the references to colour in this figure legend, the reader is referred to the Web version of this article.)

2.2.1. Rainfall scenarios

According to the index-flood approach, the design rainfall depth quantile can be expressed by means of the Intensity-Duration-Frequency (IDF) curves, which are defined as:

$$h(t_c, T) = K_T \cdot a \cdot t_c^n \tag{1}$$

where $h(t_c,T)$ is the quantile of the annual maximum rainfall depth for the duration t_c and the return period T, a and n are the scale factor and the scaling exponent, respectively, and K_T is the "non dimensional inverse frequency factor", also referred to as the "growth factor". A catchment-averaged IDF curve was needed to build a design hyetograph. To this aim, areal-averages of a and n were obtained from the Italian FlOod and Catchment Atlas (FOCA, [29]). The growth factor K_T, constant for all durations, was evaluated for the Generalized Extreme value (GEV) distribution based on the equation

$$K_T = \varepsilon + \alpha / k\left(1 - e^{-k \cdot y_T}\right) \tag{2}$$

where α, ε and k are the scale, position and shape parameters, respectively, of the GEV distribution and y_T is the Gumbel reduced variable, defined as

$$y_T = -ln[ln(T / (T-1))] \tag{3}$$

Catchment-averaged values of the GEV distribution parameters α, ε and k were again derived from the FOCA dataset ([29]), and return periods ranging from 10 to 500 years were considered.

The construction of a design hyetograph requires specifying both its duration and shape. A storm duration of 1 h was selected, as it is consistent with the expected time of concentration of the study catchment. A Chicago hyetograph ([30]) was adopted, with peak rainfall depth positioned at t = 30 min, corresponding to a centered-peak configuration.

Since no joint probability analysis of rainfall and antecedent soil moisture conditions is feasible, the flood return period is assumed to equal that of the rainfall. This assumption, commonly adopted in design practice for small ungauged catchments (e.g. Refs. [31–33]), implies that the flood response is dominated by the rainfall forcing rather than by antecedent hydrological conditions.

2.2.2. Rain-on-grid hydrodynamic model

Flood simulations are performed using a Rain-on-Grid approach, which extends depth-averaged 2D Shallow Water Equations (2D-SWE) modelling to explicitly simulate event-based rainfall–runoff processes over complex topography, without requiring a separate hydrological model to generate boundary conditions. This approach has been demonstrated to be effective for integrated hydrological–hydraulic modelling in small to medium catchments (e.g. Refs. [34–39]).

Neglecting the role of steep slope in the formulation of the governing equations ([40]), the mathematical model can be expressed in the following form Eq. (4):

$$\frac{\partial \mathbf{U}}{\partial t} + \frac{\partial \mathbf{F}}{\partial x} + \frac{\partial \mathbf{G}}{\partial y} = \mathbf{S} + \mathbf{S}_{\mathrm{RR}} \tag{4}$$

where t is time, x and y are the spatial coordinates, $\mathbf{U}$ is the vector of the conserved variables, $\mathbf{F}$ and $\mathbf{G}$ are the flux vectors in the x and y directions, $\mathbf{S}$ is the source terms describing the effects of bed slope and bed friction, and $\mathbf{S_{RR}}$ represents the effects of rainfall and infiltration rates. The vector $\mathbf{S_{RR}}$ allows one to extend the application of the 2D-SWEs modeling from the traditional river flood propagation to rainfall-runoff simulations in rural areas. The vectors reported in Equation (4) can be written as in Eq. (5):

$$\mathbf{U} = \begin{pmatrix} h \\ hu \\ hv \end{pmatrix}; \mathbf{F} = \begin{pmatrix} hu \\ hu^2 + \dfrac{gh^2}{2} \\ huv \end{pmatrix}; \mathbf{G} = \begin{pmatrix} hv \\ huv \\ hu^2 + \dfrac{gh^2}{2} \end{pmatrix}; \mathbf{S} = \begin{pmatrix} 0 \\ gh(S_{0,x} - S_{f,x}) \\ gh(S_{0,y} - S_{f,y}) \end{pmatrix}; \mathbf{S_{RR}} = \begin{pmatrix} R - I \\ 0 \\ 0 \end{pmatrix} \tag{5}$$

in which: h (m) is the water depth, u, v (m/s) are the depth-averaged flow velocities in x- and y-directions, g (m/s^2) is the gravitational acceleration, $S_{0,x}$ and $S_{0,y}$ (−) are the bed slopes in x- and y-directions, $S_{f,x}$ and $S_{f,y}$ (−) are the friction slopes in x- and y-directions, evaluated by using the Manning equation, R (m/s) is the rainfall intensity, I (m/s) represents the hydrologic losses.

The numerical model used to solve the governing equations is Tuflow HPC for GPU engine ([41]). The version uses second-order solution accuracy in space and fourth-order solution accuracy in time to solve continuity equation and momentum equations.

The use of a high-resolution, physically based SWE model is particularly suited to the cascading hazard problem addressed here for two main reasons. First, the explicit two-dimensional resolution of the flow field enables the simulation of backwater effects and local flow redistribution induced by channel obstruction, which represent the dominant mechanisms driving hazard amplification in the considered cascading scenarios. Second, because the Rain-on-Grid framework operates directly on the digital terrain model (DTM) as the computational domain, landslide-induced channel obstruction can be represented by locally modifying terrain elevations within the same domain, without the need to redefine boundary conditions or couple separate hydraulic models. This ensures that the hydrodynamic response to geomorphological modification, including backwater propagation upstream and flow redistribution across the floodplain, is resolved consistently across the entire domain, and that the comparison between baseline and modified-terrain scenarios is free from numerical artefacts at model interfaces.

Model setup details, including computational grid resolution, roughness parameterisation, boundary conditions, and initial conditions, are reported in Appendix A2.

3. Study area

The Tyrrhenian coast of Calabria was selected as the study area on the basis of four converging criteria: the presence of small steep ungauged catchments with documented geomorphological instability and torrential hydrology; a dense concentration of coastal WWTPs located in morphodynamically active floodplains; the availability of national INSPIRE-compliant datasets adequate for desk-based screening; and a documented history of cascading geo-hydrological events affecting infrastructure in the region. These characteristics make this sector of the southern Tyrrhenian coast a representative and analytically tractable setting for developing and demonstrating the proposed framework.

The study area extends along the northern Tyrrhenian coast of Calabria (southern Italy), between the Lao River basin to the north and the Savuto River valley to the south, encompassing a dense set of small catchments draining directly into the Tyrrhenian Sea (Fig. 4). The area is geologically characterised by the metamorphic and sedimentary formations of the southern Apennines, with steep mountainous headwaters transitioning abruptly to narrow coastal plains through short, confined valley reaches. Catchment areas range from less than 0.5 km^2 to approximately 65 km^2, with mean slope of the order of 30% and mean channel slopes frequently exceeding 15% in the upper course. Strong seasonal dominated precipitation regime, characterized by short-duration, high-intensity convective events in autumn and winter.

These physiographic characteristics, small basin areas, steep gradients, short flow paths, and direct hillslope-to-coast connectivity, produce very short hydrological response times and high specific peak discharges, making the lower valley reaches and coastal plains particularly prone to rapid and intense flood dynamics. The combination of active slope instability, typical of southern Apennine lithologies, and the confined channel geometries of these basins creates conditions structurally predisposed to the cascading flood–landslide interactions that this study addresses.

The area hosts 26 WWTPs, many located in lower valley reaches or near river mouths to serve coastal communities (Fig. 4). The co-occurrence of torrential hydrology, geomorphological instability, and concentration of critical wastewater infrastructure within small basins makes this sector of the Tyrrhenian coast a representative and analytically tractable setting for developing and demonstrating the hierarchical cascading hazard framework proposed here.

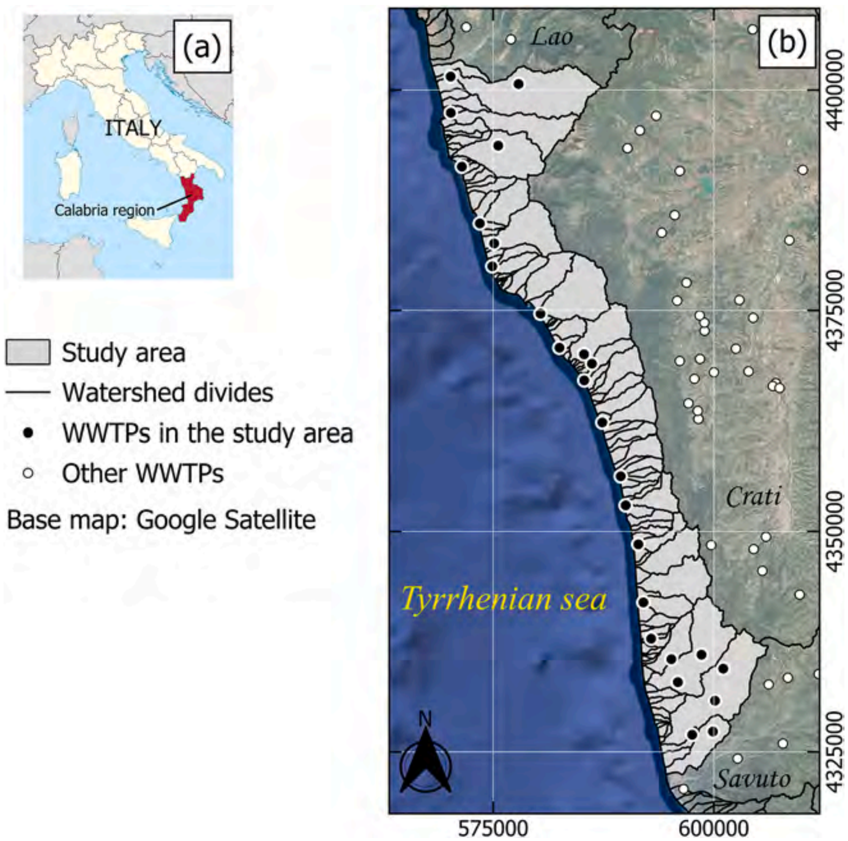

Fig. 4. Location of the study area (a) and spatial distribution of the WWTPs sites (b).

4. Results

4.1. Results of the desk-based screening and on-site verification

Application of the desk-based screening criteria to the 26 WWTPs identified along the northern Tyrrhenian coast of Calabria retained 10 sites for field inspection, with 16 excluded on the basis of absence of spatial overlap between the WWTP footprint and all three screening layers considered: flood-prone areas (any return period scenario), landslide inventory polygons, and channel-crossing infrastructure within the catchment (Fig. 5a, Table 3). Sites satisfying none of these criteria were considered as presenting no GIS-detectable basis for cascading hazard activation. Notably, none of the analysed facilities are located within mapped landslide areas.

Field inspections of the 10 retained sites allowed further classification and exclusion. Sites exhibiting robust perimeter protection or sufficient freeboard to preclude meaningful hazard–facility interaction were excluded from further analysis. Among the remaining sites, two were assigned to category C1, three to category C2, and one to category C3 (Table 3, Fig. 5b).

The Maddalena catchment, within the municipality of Fuscaldo and the only site classified as C3, was selected as demonstrator for full cascading hazard modelling, as it exhibits the simultaneous presence of all predisposing factors defining the multi-pathway cascading configuration. Field evidence supporting this classification is collectively illustrated in Fig. 6: a road crossing with limited freeboard immediately downstream, (Fig. 6b and c), an active or relict landslide on the left channel bank (Fig. 6d), and a WWTP in close proximity to the channel with components at low elevation relative to the surrounding terrain (Fig. 6e) with vulnerable components situated in areas potentially exposed during high flow conditions, as documented by the images from the most recent flood event (Fig. 6f).

The WWTP at the Maddalena site is designed to treat 15,000 population equivalents (PE), configured into three parallel treatment lines of 5000 PE each. The facility comprises three functional units (Fig. 7): mechanical and biological pre-treatment (Unit 1), biological treatment tanks (Unit 2), and a sludge treatment line (Unit 3), which includes drying beds, a flotation section, and a mechanical dewatering unit. Units 1 and 2 are founded at elevations between +2.10 and + 4.50 m above ground level. Unit 3, and specifically the sludge drying beds, occupies the lowest portion of the plant, at approximately +0.50 m above ground level, making it the most hydraulically exposed component of the facility under flood conditions. The implications of this elevation for flood impact assessment are discussed in Section 4.2.

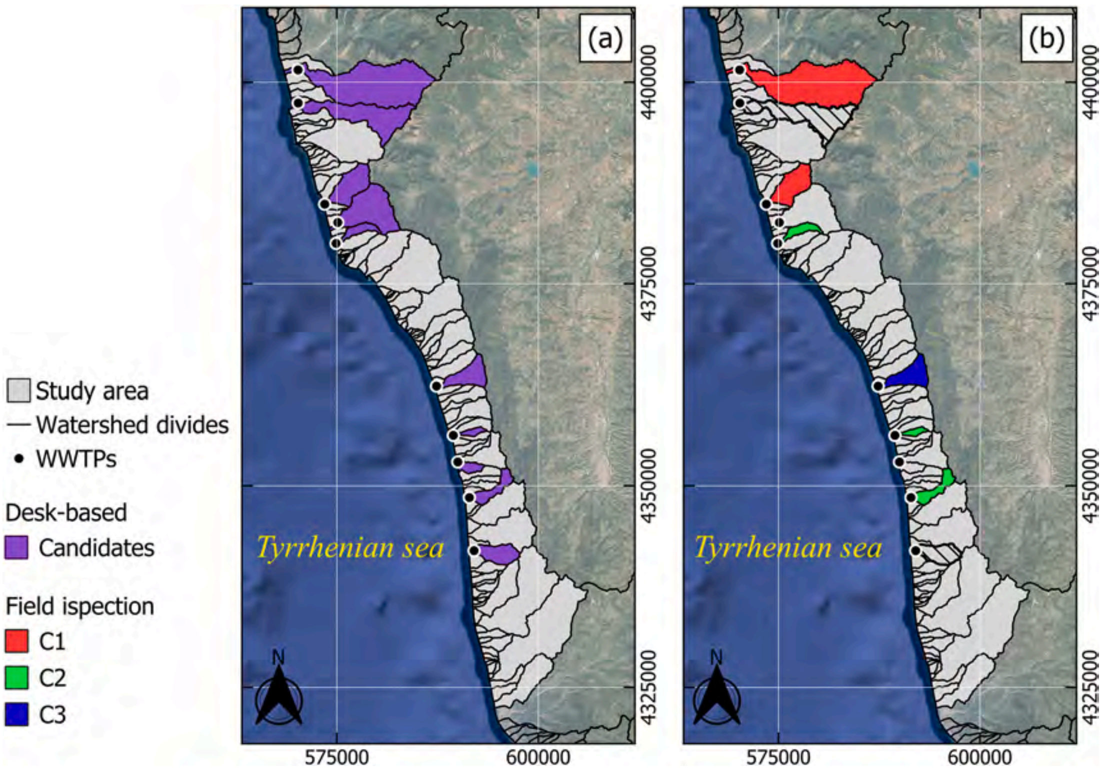

Fig. 5. Results of the large-scale screening and field verification. Panel (a) illustrates the outcome of the desk-based screening, showing only hazard prone coastal WWTPs. Panel (b) shows the spatial distribution of sites classified into three potential cascading-hazard categories based on field inspections (C1: red; C2: green; C3: blue). Black diagonal line patterns indicate sites with negligible hazard-facility interaction based on field inspection.

Table 3
Summary of the stepwise screening process, including desk-based analysis and field verification, with the number of sites excluded and retained at each stage.

Screening stage	N. sites	Excluded	Retained	Reason for exclusion
Initial WWTPs	26	-	26	-
STEP 1: desk-based	26	16	10	No hazard overlap
STEP 2: Field verification	10	6	4	Negligible interaction
Classification C1	-	-	2	
Classification C2	-	-	1	
Classification C3	-	-	1	

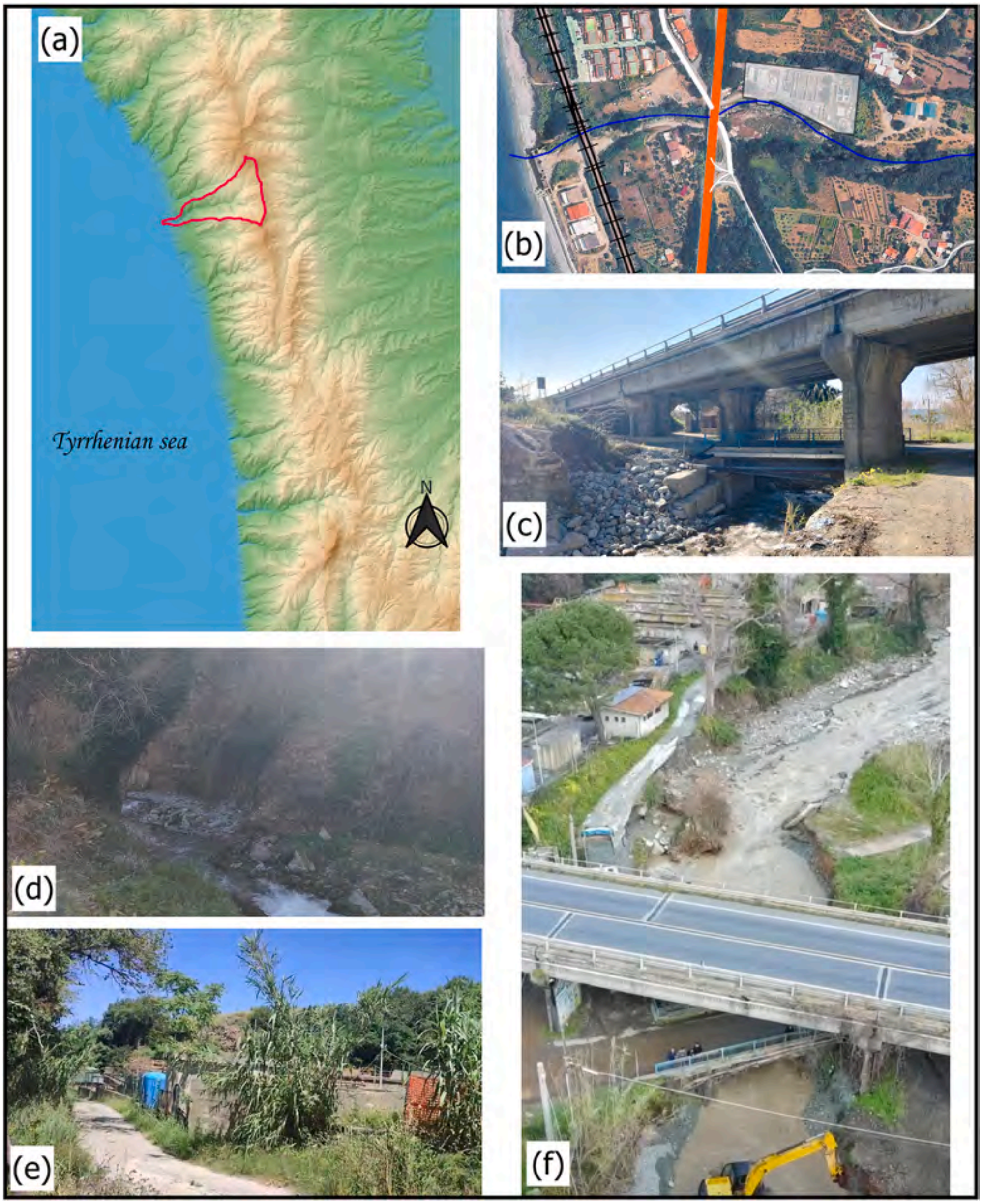

Fig. 6. Field inspection evidence supporting the C3 classification of the Maddalena catchment, located in the municipality of Fuscaldo. (a) Location of the catchment along the northern Tyrrhenian coast of Calabria; (b) overview of the study reach showing the road crossing, railway infrastructure, and WWTP position; (c) road crossing with limited freeboard over the active channel; (d) unstable left-bank slope with active erosional processes and sparse vegetation cover; (e) WWTP site in close proximity to the channel; (f) aerial view of post-flood restoration works following the event of 13 February 2026, documenting the hydraulic connectivity between the channel and the WWTP area.

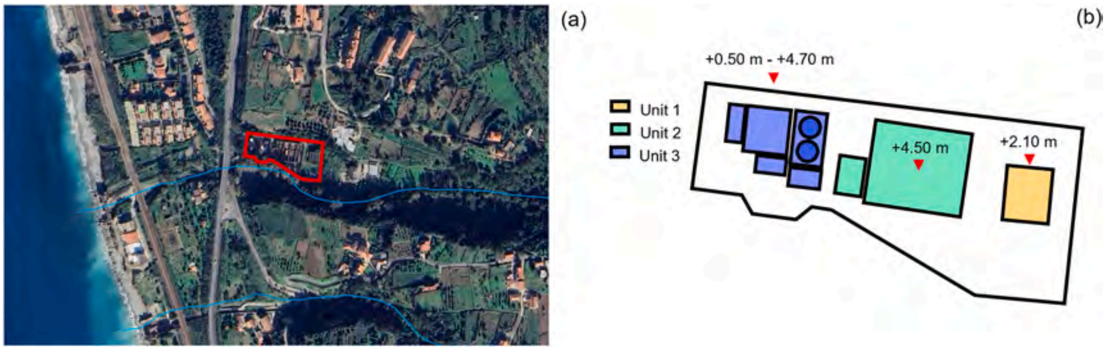

Fig. 7. Location of the wastewater treatment plant (a) and layout of its units, with elevations (b).

4.2. Flood hazard amplification under cascading scenarios

The following results are organised in two parts. The first presents the hydrodynamic outcomes of the three modelled scenarios, A (clear-water), B (uniform deposit), and C (channel-concentrated deposit), with a focus on the spatial distribution of water depths and velocities within the study reach. The second presents the sensitivity analysis of the cascading hazard outcome to landslide volume, establishing the threshold reduction required to maintain water depths below the critical elevation of the most exposed WWTP components.

The sludge drying beds of Unit 3, located at approximately +0.50 m above ground level (Section 4.1), represent the most hydraulically exposed components of the facility. Exceedance of this elevation by simulated water depths is used as the operational threshold for cascading hazard activation, the condition under which overtopping of the drying beds and potential sludge mobilisation may occur. All results are therefore interpreted with reference to this threshold.

Fig. 8 shows the longitudinal cross-section at the WWTP location (cross-section 1-1′, Figure A3) under baseline topographic conditions and under the two modified DTM configurations. The introduction of a uniform 2.5 m deposit across the channel cross-section (Scenario B, estimated in Appendix A1) substantially reduces conveyance capacity relative to the baseline. The channel-concentrated deposit (Scenario C), applied at a constant elevation of 4.5 m from the thalweg, produces a flattening of the cross-sectional geometry that extends the inundated area over the left floodplain. Both configurations represent physically plausible end-members of post-landslide sediment redistribution, as discussed in Section 2.2.

Fig. 9 compares the spatial distribution of maximum simulated water depths for a 200-year return period rainfall event under Scenario A and Scenarios B and C. Under Scenario A, the 200-year flood does not reach Unit 3 of the WWTP, including the sludge

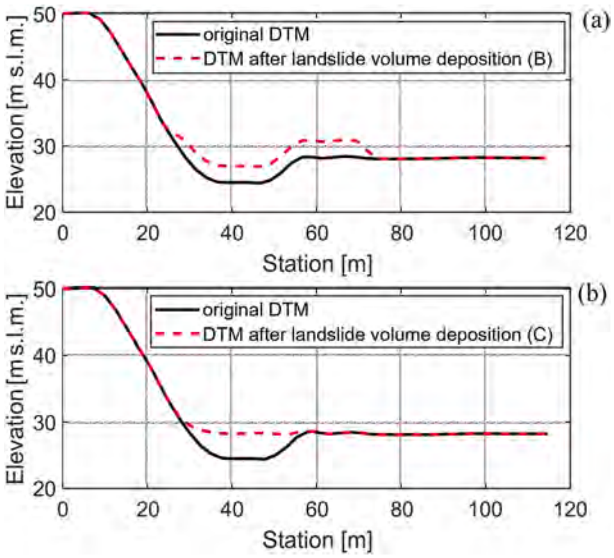

Fig. 8. Typical cross-section in current conditions and modified to include a uniformly distributed 2.5 m deposit across the channel and floodplain (a); typical cross-section in current conditions and modified to include a 4.5 m deposit from the channel bed (b).

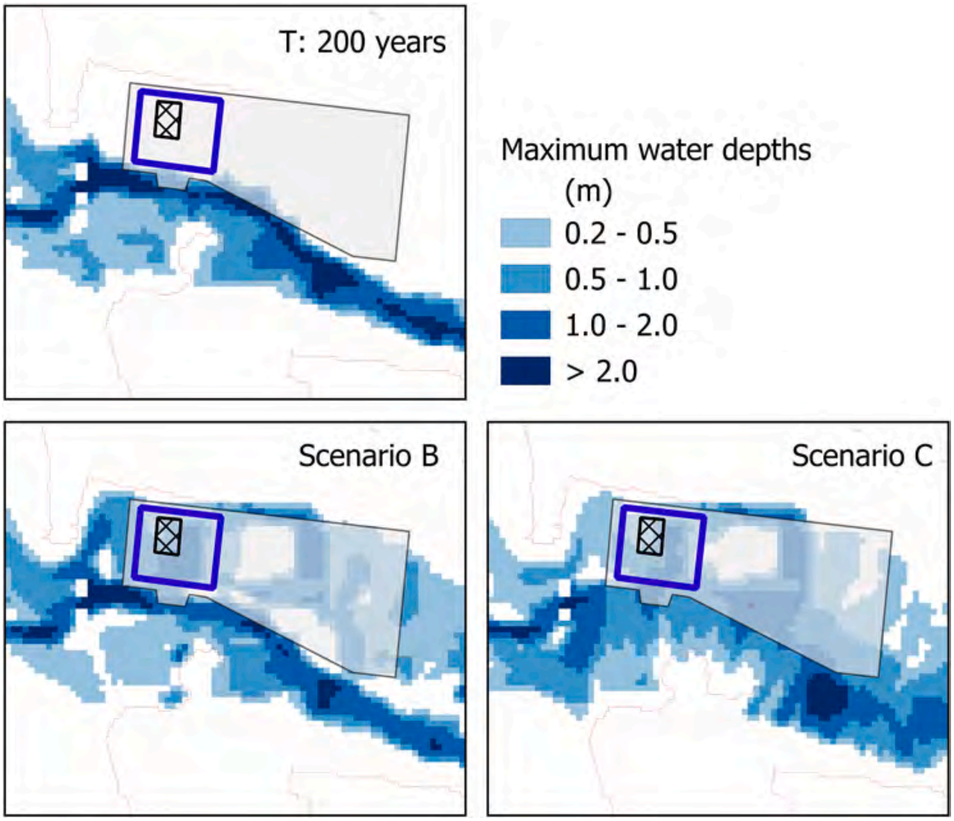

Fig. 9. Spatial distribution of water depths within the study area for a 200-year return period rainfall event under the clear water scenario and the two cascading hazard configurations (flood scenarios B and C).

drying beds. The introduction of landslide deposits in Scenarios B and C substantially modifies flow routing: backwater effects propagate upstream of the obstruction, generating localised ponding in the area immediately adjacent to the WWTP. This spatial redistribution of inundation is accompanied by a marked reduction in flow velocities relative to Scenario A (Fig. 10), consistent with the energy dissipation associated with flow constriction and upstream storage.

The hydrodynamic impact on Unit 3 under the two cascading scenarios is quantified in Table 4, which reports spatially averaged maximum water depth, flow velocity, and bed shear stress within the unit footprint. Under both Scenario B and Scenario C, the spatial mean, maximum, and 90th percentile water depths exceed the 0.50 m threshold, indicating that cascading conditions activate the critical flood exposure of the sludge drying beds under a 200-year rainfall event, a return period under which the facility remains entirely unaffected in the clear-water scenario.

To identify the minimum return period required to activate cascading hazard, Fig. 11 presents maximum water depth maps for Scenario C, the less severe of the two deposit configurations in terms of impact on Unit 3, under rainfall events with return periods below 200 years. Results show that the 0.50 m threshold is exceeded for return periods as low as approximately 50 years, representing a reduction of one order of magnitude relative to the clear-water scenario in which the facility remains unaffected even under 500-year return-period rainfall.

The sensitivity of this threshold to landslide volume is assessed in Fig. 12, which presents the 90th percentile water depth simulated at Unit 3 across a matrix of return periods and landslide volume fractions relative to the reference estimate. Red cells indicate scenarios in which the 0.50 m threshold is exceeded.

Results show that cascading hazard activation persists across a wide range of volume reductions: even when the mobilised volume is reduced to 60% of the reference estimate, corresponding to a 40% reduction, the threshold is exceeded for return periods exceeding 50 years. A reduction to 50% of the reference volume is required to maintain water depths below the critical threshold across all return periods considered. These findings demonstrate that the order-of-magnitude shift in hazard return period is a robust feature of the cascading mechanism, not an artefact of the specific volume assumption.

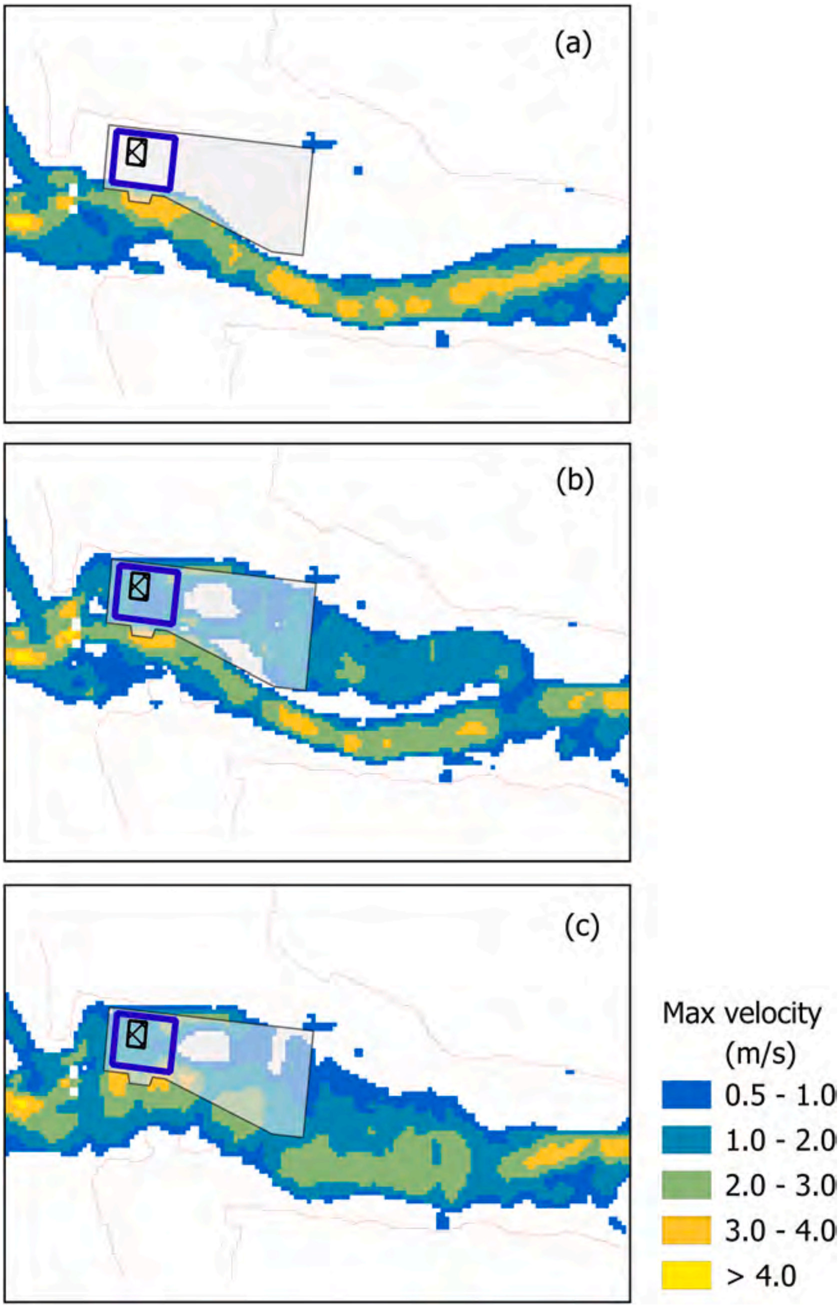

Fig. 10. Spatial distribution of flow velocity within the 200-year return period rainfall event under the clear water scenario (a) and the two cascading hazard configurations B and C (b, c).

Table 4
Spatially averaged maximum water depths, flow velocities, and bed shear stresses for Unit 3 of the wastewater treatment plant under the two landslide-deposit configurations: (B) uniform deposit and (C) channel-concentrated deposit.

Mean (m)		Max (m)		90th percentile (m)	
(B)	(C)	(B)	(C)	(B)	(C)
0.8	0.7	1.8	1.6	1.2	1.1

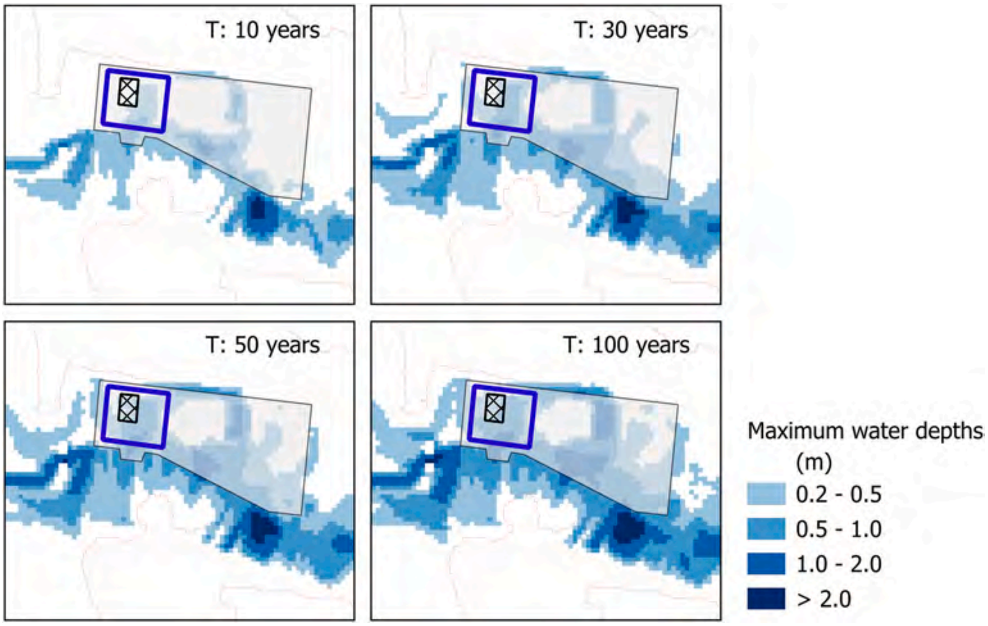

Fig. 11. Maximum depth maps under landslide-flood cascading for rainfall scenarios with return periods, below 200 years. Flood scenario C.

Fraction of landslide volume (-) \ Flood return period (years)	10	30	50	100	200	300	500
1	0.46	0.66	0.78	0.93	1.06		
0.85			0.47	0.61	0.77		
0.7				0.31	0.45	0.52	0.66
0.6						0.45	0.55
0.5						0.33	0.44

Fig. 12. Matrix of the 90th percentile water depths simulated at Unit 3 for varying return periods and landslide volume fractions. Red cells indicate activation of sanitary hazard (depth >0.5 m). The analysis shows that despite volume reductions, hazard persists at return periods lower than those required for clear-water flooding. A volume reduction to 0.5–0.6 of the original mass is required to maintain depths below the critical threshold.

5. Discussion

The results demonstrate the effectiveness of the hierarchical framework across both its components. At the screening stage, the stepwise application of desk-based criteria and field inspections systematically identified the sole site exhibiting the physical preconditions for multi-pathway cascading hazard activation, concentrating analytical effort where it is most warranted. At the modelling stage, cascading hazard simulation reveals that landslide-induced channel obstruction produces an order-of-magnitude reduction in the flood return period required to inundate the most vulnerable WWTP components, a shift that is robust across sediment distribution configurations and persists under substantial landslide volume reductions.

These findings have two distinct implications. First, the hierarchical screening framework can systematically identify, at regional scale, catchment–infrastructure configurations predisposed to cascading hazard activation that would remain undetected by desk-based analysis alone. Second, static multi-hazard overlay approaches substantially underestimate flood hazard at sites where geomorphological system state changes, invisible to independent hazard assessments, govern the dominant impact pathway. The following discussion addresses these implications in sequence: screening performance and transferability (Section 5.1), cascading hazard modelling and its comparison with multi-hazard overlay (Section 5.2), before drawing broader conclusions for risk management and future research (Section 5.3).

5.1. Screening framework: performance, implications, and limitations

Of the 26 WWTPs analysed along the Tyrrhenian coast, 10 were retained after desk-based screening and 6 after field inspection, with only one site, the Maddalena catchment, exhibiting the multi-pathway cascading configuration that warrants full process-based modelling. This stepwise reduction from 26 to 10 to 6 to 1 site demonstrates that the hierarchical structure of the framework concentrates analytical effort efficiently: desk-based screening eliminates 62% of sites using only publicly available data, field inspection eliminates a further 40% of retained sites on the basis of observable protective measures and freeboard, and the C1/C2/C3 classification prioritises the sole C3 site for full cascading hazard modelling. This progressive filtering confirms that configurations predisposed to cascading flood–landslide interaction affecting WWTPs are not ubiquitous but are identifiable through a structured, criteria-based protocol. Sites classified as C1 and C2 are not excluded from risk management: they retain hydraulic exposure through the mechanisms described in Table 2 and are forwarded to standard hydraulic assessment. Only C3 sites require the full cascading modelling framework, concentrating the associated computational effort where it is physically warranted.

The framework is designed to be transferable to any coastal setting where small ungauged catchments host critical wastewater infrastructure in proximity to geomorphologically active channels. The physiographic characteristics that define the framework's applicability — steep ungauged catchments, geomorphologically active slopes, confined channel geometries, and coastal critical infrastructure — are widespread across the Mediterranean region, including large sectors of the southern Italian, Greek, French and Spanish coastlines.

Three conditions are necessary for its application. First, publicly available regional datasets, flood hazard maps, landslide inventories, and georeferenced infrastructure locations, must be available at sufficient resolution to support desk-based screening; in the European context, INSPIRE-compliant national datasets satisfy this requirement in most member states. Second, field inspection must be feasible to verify and classify retained sites, a step that, while requiring expert geomorphological and hydraulic judgement and implying a non-negligible time investment, remains relatively low-cost compared to full process-based modelling as it demands no computational infrastructure or bespoke instrumentation. Third, a two-dimensional hydrodynamic model capable of rain-on-grid simulation and DTM modification must be available for the priority catchment; several open-source and commercial platforms now provide this capability.

At the regional screening stage, the desk-based criteria are deliberately conservative and rely on datasets that do not capture actual channel conveyance capacity, current hydraulic structure condition, or the presence of local protective measures. These limitations motivate the field inspection step but also mean that the screening cannot be fully automated. The C1/C2/C3 classification addresses a defined subset of cascading configurations; other mechanisms, including debris blockage of bridge openings, progressive bank erosion, or sediment aggradation from multiple upstream sources, can generate comparable backwater effects and warrant extension of the classification scheme in future applications. It should be observed that the C1/C2/C3 classification

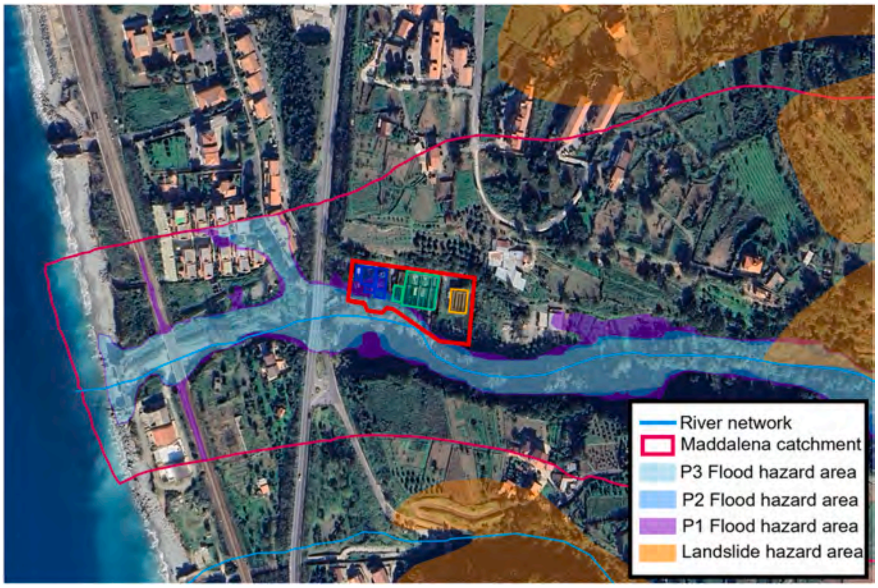

Fig. 13. Overlay of national flood and landslide hazard maps with the locations of the WWTP units in the Maddalena stream basin, i.e. Unit 1 (in orange), Unit 2 (in green), Unit 3 (in blue).

describes dominant interaction mechanisms rather than absolute hazard severity: in catchment contexts where landslide-channel connectivity is absent but hydraulic constriction or limited infrastructure freeboard are critical, a C1 or C2 site may represent the highest-priority configuration for risk management and should be assessed accordingly.

5.2. Cascading hazard modelling: what multi-hazard overlay misses and why

Overlaying the national flood and landslide hazard maps with the WWTP unit locations (Fig. 13) shows that, under a conventional multi-hazard approach, Unit 3 falls within the low-probability flood hazard zone (P1, T = 500 years) and outside all mapped landslide-prone areas. This assessment would lead to the conclusion that the sludge drying beds are exposed only under extreme, low-probability events, and that no landslide-related hazard pathway exists at the site. Both conclusions are incorrect under cascading conditions.

The cascading hazard analysis reveals that Unit 3 is inundated beyond the critical threshold under an approximately 50-year rainfall event when a landslide-induced channel obstruction is present, corresponding to a return period ten times shorter than that suggested by the official flood hazard map, and a hazard pathway entirely absent from the landslide inventory. This discrepancy arises not from deficiencies in the official maps, which are fit for their intended purpose, but from a structural limitation of the static overlay approach: by treating flood and landslide hazards as independent, it cannot represent the hydraulic consequences of geomorphological system state changes. The backwater effect generated by channel obstruction is not a flood hazard in isolation, nor a landslide hazard in isolation, it is an emergent property of their physical interaction, and is therefore invisible to any assessment that evaluates the two hazards separately. It is worth noting that this structural limitation is independent of inventory completeness: had the landslide visible in Fig. 6d been included in the official inventory, a spatial overlay approach would have identified its proximity to the WWTP and flagged the site as potentially vulnerable, but would still have been unable to capture the backwater mechanism and the resulting order-of-magnitude reduction in critical flood return period, which emerges only from the physical interaction between geomorphological state change and flood dynamics. This finding is consistent with the broader literature on cascading hazard amplification in confined catchments ([20]), and extends it to the specific context of critical wastewater infrastructure in ungauged coastal basins. The magnitude of the return period shift identified here, one order of magnitude, is at the upper end of what has been reported for geomorphologically driven flood amplification, suggesting that small steep catchments with confined channel geometries and low infrastructure freeboard may be particularly susceptible to this class of cascading interaction.

The observed reduction in rainfall return period should therefore be interpreted conditionally, i.e., as the rainfall threshold required to trigger critical inundation given a pre-existing channel obstruction. Extending the framework toward fully probabilistic cascading risk estimates would require modelling landslide occurrence frequency and rainfall–landslide dependence structures, which lie beyond the scope of the present hazard-focused analysis.

The hydrodynamic model was not calibrated or validated against observed flood events, due to the absence of reliable discharge records and documented inundation data in the ungauged study catchment. This limitation is consistent with the data-scarce conditions that characterise many small coastal basins. The modelling approach adopted here is therefore scenario-based and process-oriented, and does not aim to provide predictive flood hazard estimates. Instead, it focuses on the relative change in flood behaviour induced by landslide-driven channel obstruction, by comparing clear-water and obstruction scenarios under consistent boundary conditions. Within this framework, the identification of cascading hazard activation and the associated shift in return period should be interpreted as a physically plausible response of the system to geomorphological perturbation, rather than as an absolute prediction of flood magnitude.

At the local modelling stage, landslide volumes were estimated through a simplified inventory-based procedure without field measurement or empirical calibration against observed events. While the sensitivity analysis demonstrates that the cascading mechanism is robust to volume reductions of up to 40%, the adopted landslide volume estimates are further supported by their consistency with the empirical area–volume relationship proposed by Ref. [42], derived from a worldwide catalogue of 677 slide-type landslides. The landslide area–volume pairs considered in this study fall within the expected range of this established scaling relationship, thereby increasing confidence in the adopted volume assumptions. The landslide trajectories remain a possible source of uncertainty that future work should address. While the adopted deposits configurations represent simplified end-members, they are intended to define a physically plausible envelope of channel obstruction scenarios, rather than to reproduce a specific historical event. More complex deposition patterns, including complete blockage or highly heterogeneous spatial distributions, were not considered but may further influence flow dynamics and warrant investigation in future applications of the framework developed in this paper.

The assumption that landslide deposits are pre-existing at the onset of the flood event simplifies the temporal dynamics of the cascading sequence and does not account for the probability of hazard co-occurrence, which varies with the local climatic and geomorphological regime. It is important to note that the analysis is scenario-based: it does not establish the probability of co-occurrence of the landslide and flood events, nor does it quantify the resulting sanitary or environmental risk. Rather, it identifies the threshold conditions under which cascading hazard activation becomes physically possible, a necessary precondition for any subsequent risk quantification.

5.3. Implications for risk management

From a risk management perspective, the gap between static regulatory hazard classifications and interaction-driven cascading hazard, as illustrated by this study, is not merely conceptual: under the current regulatory framework, the Maddalena WWTP would not be identified as a priority site for cascading hazard mitigation, since its most vulnerable components fall outside the landslide hazard zone and are classified as exposed only under low-probability flood events. The cascading analysis demonstrates that this classification substantially underestimates the actual hazard exposure of the facility. Integrating scenario-based cascading assessments into national flood risk management plans would provide a more complete basis for infrastructure protection prioritisation, particularly for critical facilities located in morphodynamically active floodplains.

From an operational risk management perspective, the results support targeted monitoring of upstream channel constrictions, unstable slopes, and critical hydraulic controls that may amplify flood impacts on sensitive infrastructure. The C1/C2/C3 classification provides a practical basis for prioritising inspection and maintenance resources across multiple sites without requiring full cascading hazard modelling at each location. Sites classified as C3 warrant periodic monitoring of channel morphology and slope stability, with particular attention to conditions, such as antecedent rainfall, vegetation loss, or seismic activity, that may precondition landslide delivery to the channel network.

Overall, the scenario-based cascading assessments demonstrated here should be integrated into the next revision cycle of Flood Risk Management Plans under the EU Floods Directive (2007/60/EC). Current FRMPs are predominantly based on single-hazard flood maps that do not account for geomorphological state changes; incorporating cascading hazard screening as a mandatory step for critical infrastructure located in morphodynamically active catchments would provide a more complete basis for infrastructure protection prioritisation at the national and river basin district level.

Finally, although demonstrated for wastewater treatment plants, the hierarchical framework is directly transferable to other categories of critical infrastructure located in small coastal catchments, including pumping stations, industrial facilities, hospitals, and road or rail infrastructure crossing active channels. The C1/C2/C3 classification scheme and the cascading modelling approach are applicable to any configuration where geomorphological and hydraulic connectivity between upstream slopes and downstream infrastructure creates conditions for hazard amplification beyond what single-hazard assessments can detect.

6. Conclusions and future research directions

This study proposed and demonstrated a hierarchical stepwise framework for identifying and assessing cascading geo-hydrological impact pathways threatening wastewater treatment plants in small steep ungauged coastal catchments. The framework operates through three progressive steps: desk-based regional screening, targeted field inspections, and two-dimensional rain-on-grid hydrodynamic modelling, with DTM modification, designed to concentrate analytical effort on the subset of sites where cascading hazard activation is physically predisposed.

Applied to 26 WWTPs along the Tyrrhenian coast of Calabria, the screening protocol systematically reduced the candidate pool from 26 to 10 sites through desk-based criteria, and from 10 to 1 through field inspection and C1/C2/C3 classification, identifying the Maddalena catchment as the sole site exhibiting multi-pathway cascading potential. This progressive filtering demonstrates that configurations predisposed to cascading hazard activation are identifiable at regional scale through a structured, low-cost protocol, without requiring detailed hydraulic modelling at every site. The transferability of the framework depends on three conditions that are broadly satisfied in European coastal contexts: availability of INSPIRE-compliant regional hazard and infrastructure datasets, feasibility of expert field inspection, and access to a two-dimensional hydrodynamic modelling platform.

Process-based cascading hazard modelling at the Maddalena catchment demonstrates that landslide-induced channel obstruction generates backwater effects that reduce the flood return period required to inundate the sludge drying beds of the WWTP from beyond 500 years under clear-water conditions to approximately 50 years under cascading conditions, a shift of one order of magnitude. This threshold shift persists across both sediment distribution configurations modelled and under landslide volume reductions up to 40%, confirming that the result is a robust feature of the cascading mechanism rather than an artefact of specific modelling assumptions. Under a conventional multi-hazard overlay approach, the same facility would be classified as exposed only under low-probability extreme events and as unaffected by landslide hazard, both conclusions that cascading modelling demonstrates to be incorrect.

The exceedance of the 0.50 m elevation threshold at Unit 3 under cascading conditions provides a conservative operational proxy for the onset of sludge mobilisation and potential environmental contamination. This hazard-based criterion is consistent with the scenario-based and decision-support nature of the framework, and is particularly suited to data-scarce environments where damage functions and contamination transport models are unavailable. Translating the hazard-based findings presented here into quantitative risk estimates, incorporating damage functions for WWTP components, contamination transport modelling in the downstream fluvial and coastal environment, and exposure assessment of human receptors, represents the most impactful direction for future research.

From a risk management perspective, the results support three operational recommendations. First, WWTPs and analogous critical facilities located in small coastal catchments with geomorphologically active upstream slopes should be systematically screened using the hierarchical protocol proposed here, prioritising sites where landslide proximity, channel-crossing infrastructure, and low facility freeboard co-occur. Second, monitoring programmes should target upstream channel constrictions, unstable slopes, and hydraulic controls capable of generating backwater effects, elements that are not captured by standard flood or landslide hazard maps but that control cascading hazard activation. Third, scenario-based cascading assessments should be integrated into national flood risk management plans to provide a more complete basis for infrastructure protection prioritisation under the EU Floods Directive framework.

More broadly, this study demonstrates that the gap between site-specific cascading process understanding and regional risk screening is bridgeable through a structured hierarchical approach that does not require instrumented catchments, extensive field campaigns, or bespoke modelling infrastructure. As geomorphological instability and hydrometeorological extremes intensify under changing climatic conditions, systematic identification of latent cascading impact pathways on critical infrastructure will become an increasingly essential component of flood risk management in coastal environments.

Declaration of generative AI use

During the preparation of this work, the authors made partial use of AI-assisted technologies (ChatGPT) to improve readability and language. All content generated with the help of this tool was reviewed and edited by the authors, who take full responsibility for the final version of the manuscript.

Funding

This study was carried out within the RETURN Extended Partnership and received funding from the European Union Next-GenerationEU (National Recovery and Resilience Plan – NRRP, Mission 4, Component 2, Investment 1.3 – D.D. 1243 2/8/2022, PE0000005 - Spoke TS 2).

CRediT authorship contribution statement

Margherita Lombardo: Formal analysis, Software, Validation, Writing – original draft, Writing – review & editing. **Giulia Evangelista:** Data curation, Formal analysis, Validation, Writing – original draft, Writing – review & editing. **Pierluigi Claps:** Funding acquisition, Methodology, Project administration, Supervision, Validation, Writing – review & editing. **Pierfranco Costabile:** Conceptualization, Investigation, Methodology, Supervision, Writing – original draft, Writing – review & editing.

Declaration of competing interest

The authors declare that the research was conducted in the absence of any commercial or financial relationships that could be construed as a potential competing interest. This work was supported by the European Commission.

Acknowledgments

The authors wish to thank Michele Torregrossa and Maria Castiglione for their support in providing data and technical information on the wastewater treatment plant in the Maddalena catchment.

Appendix

A1. Landslide volume estimation

Operating in an ungauged and data-limited context necessitated a pragmatic yet physically grounded approach. Under these constraints, the volume of potentially mobilisable landslide material was estimated through a simplified inventory-based method.

Landslide source areas were identified from the Italian Landslide Inventory (IFFI, data available at: idrogeo.isprambiente.it/app/pir, last access: 03/02/2026), including both individual rotational/translational landslides and areas affected by diffuse shallow instabilities. Landslide depth was assumed equal to the local soil thickness, estimated using the Saulnier equation ([43,44]) and mapped on a 4×4 m grid. Landslide volumes were then computed as the product of soil thickness and grid cell area within the mapped landslide polygons.

To reduce potential overestimation associated with assuming simultaneous activation and full sediment delivery, a spatial filtering procedure was applied. Only landslides located within 1 km of the river reach of interest and within a 25 m buffer from the river network were retained, under the assumption that sediment delivery is primarily controlled by proximity to the channel. The polygon area intersecting landslide bodies, approximately $4 \times 10^4\,m^2$, corresponds to a landslide volume of approximately $9 \times 10^4\,m^3$.

These assumptions are necessarily heuristic in ungauged contexts characterized by the absence of site-specific geomorphological observations. However, it should be noted that this value is fully consistent with the empirical area–volume relationship proposed by Ref. [42]: the estimated landslide volume falls well within the range of values highlighted by the empirical scatter of the 677 slide-type landslides used to derive the relationship, thus supporting the plausibility of the adopted volume.

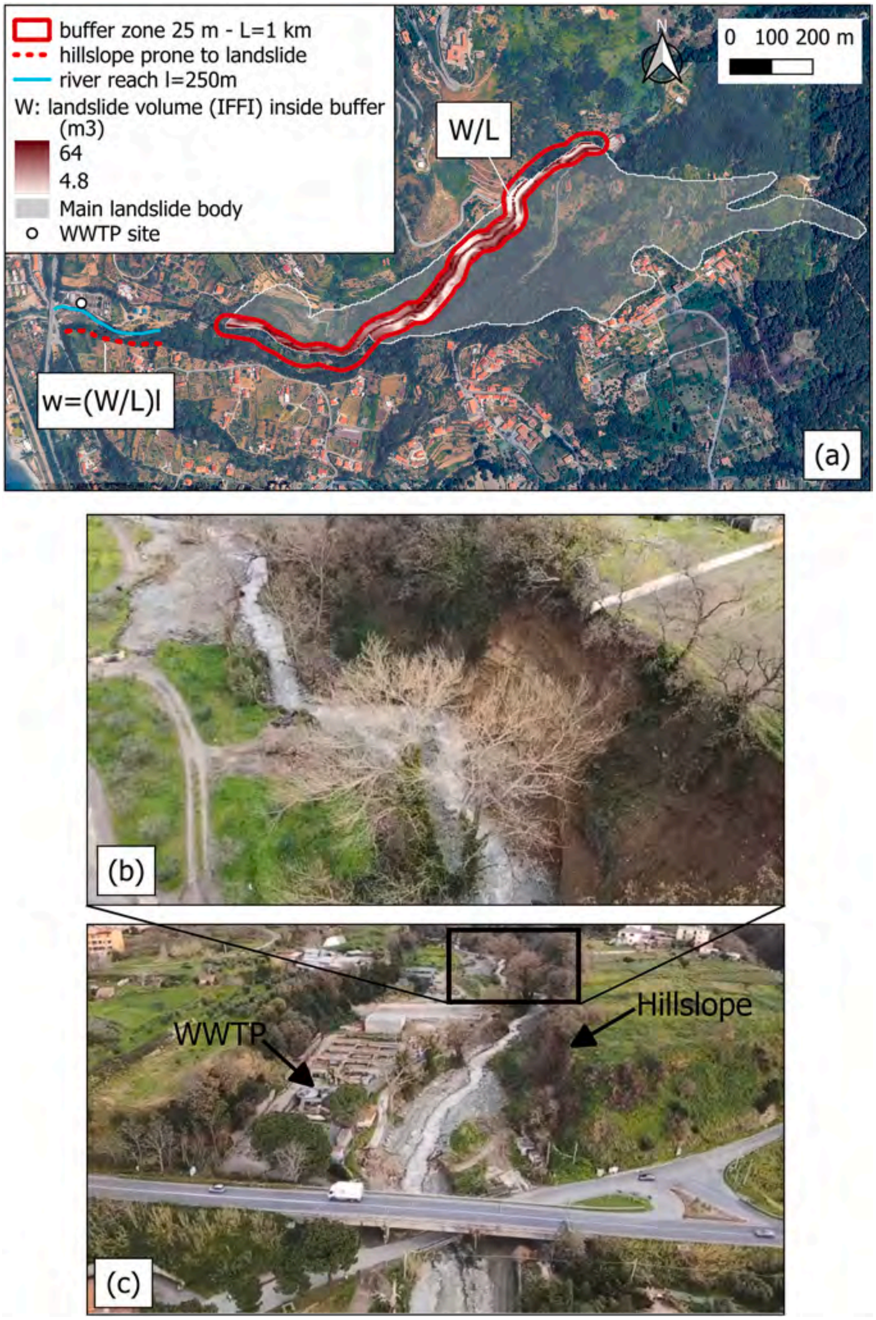

Fig. A1. Conceptual scheme of the simplified approach used to estimate potentially mobilisable landslide volumes from the hillslope outlined by the red dashed line. Sediment input is assumed to be constant per unit upstream channel length and is derived from IFFI landslide volumes located within a 25 m buffer along a 1 km upstream river reach. (b) top view of the unstable hillslope and (c) panoramic view of the wastewater treatment plant on the right hydraulic side, river channel, and the slope on the left hydraulic side.

For model implementation, a constant sediment volume per unit channel length was adopted and applied along a 250 m reach at the foot of the unstable left hillslope (Figure A1), as identified during field verifications (see section 4.1) and as recognizable from publicly available videos. Deposition thickness was derived from a depth–volume relationship representative of the analysed river reach, assuming complete deposition of the selected sediment volumes. While real debris deposition patterns are typically heterogeneous, the uniform distribution assumption allows isolating the hydraulic effect of channel aggradation without introducing additional spatial variability parameters. Localised thicker accumulations would likely produce even stronger backwater effects at specific cross-sections.

Full mobilisation of the mapped landslide mass was assumed as an upper-bound scenario to test the maximum hydraulic amplification potential associated with channel obstruction.

This estimation is affected by great uncertainty; indeed, due to the lack of site-specific data, a highly simplified, yet reasonable procedure was adopted. To account for the effects of these inherent simplifications on model outcomes the mobilised landslide volume, which was progressively reduced with respect to the initial estimate to identify the threshold below which channel morphology and flood response remain comparable to the undisturbed configuration, across different rainfall return periods.

A2. Hydrodynamic model setup

The basin scale computational domain for the Maddalena catchment consists of about $2 \cdot 10^6$ squared cells of 6 m^2 resolution, providing an adequate representation of channel geometry within the valley reach. Simulations were performed using the TUFLOW HPC GPU engine, which exploits graphics processing unit (GPU) acceleration to handle large computational domains efficiently. Each simulation required approximately 30 min on an NVIDIA RTX 4500 Ada Generation GPU, achieving a real-time to computational-time ratio of up to 6, making the approach feasible on high-end workstations without access to dedicated HPC cluster. For the domain size considered here, a workstation with a current-generation GPU would be sufficient, making the approach accessible to practitioners without HPC infrastructure.

Distributed model inputs include rainfall forcing and spatially distributed surface roughness coefficients. Gross rainfall was defined at a 5-min time step (Figure A2a). Losses due to initial abstraction ($Ia = \lambda S$) and infiltration were estimated using the SCS Curve Number method, assuming wet antecedent moisture conditions (AMC III). The Curve Number value (CN = 73) was derived from the CN map provided by Ref. [29] while $\lambda = 0.15$ is assumed for the initial abstraction coefficient. The resulting net rainfall (Figure A2b) was applied uniformly across the entire computational domain.

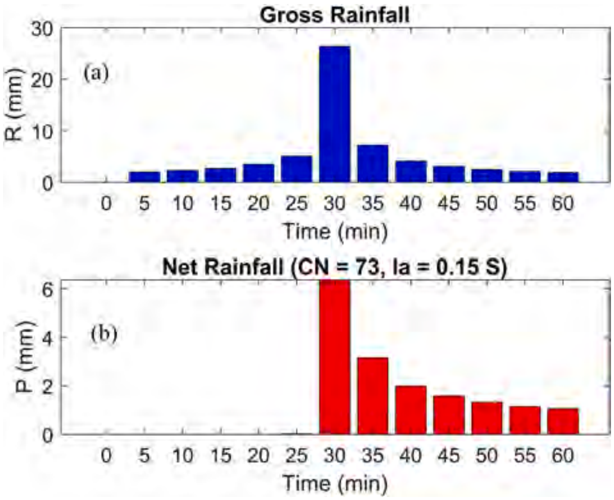

Fig. A2. Gross (a) and net hyetograph (b) with a 5-min time step.

Land cover information from the CORINE Land Cover 2018 dataset was used to define the spatial distribution of Manning's roughness coefficient. Since the CORINE dataset includes only major rivers, it was integrated with an additional polygon representing the main channel network.

A uniform Manning's coefficient of $n = 0.05\ \mathrm{s\,m^{-1/3}}$ was assigned to the main channel, while roughness values for hillslopes and floodplain areas were assigned according to land cover classes and commonly adopted ranges in rainfall–runoff applications (Table A2, cfr. [45–49]). As mentioned in Section 2, a sensitivity analysis on surface roughness parameters was performed. Detailed results, including quantitative comparisons and parameter ranges, are provided in Appendix A3.

Table A2
Manning's coefficient ranges for rainfall-runoff applications.

Land cover type	Manning's coefficient [min-max] ($s/m^{1/3}$)	Values assumed in this study ($s/m^{1/3}$)
Roads and open buid-up spaces	[0.011 – 0.025]	0.02
Green fields/grassland	[0.03 – 0.15]	0.1
Bare land	[0.03-0.06]	0.05
Mountain/hillslope/forest	[0.1-0.4]	0.1
Water bodies	[0.035 – 0.078]	0.05

Free outflow boundary conditions were applied along the entire perimeter of the computational domain. The simulations assumed a dry channel bed as the initial condition, and buildings were not explicitly represented in the hydraulic model. The hydraulic effects of the road bridge and local bank protections were approximated by introducing rows of non-floodable cells at the bridge cross-section, effectively reproducing flow constriction. Simulations were run over a total duration of 3 h, encompassing both the flood's rising and recession phases.

A3. Sensitivity to hydrological losses and surface roughness

A major source of uncertainty in the modeling arises from soil parameters, including both hydrological losses and surface roughness. To assess their influence on the model results, a sensitivity analysis was carried out by varying the key parameters around the reference configuration. For the initial abstraction coefficient λ, two additional values were tested ($\lambda = 0.10$ and $\lambda = 0.20$) alongside the reference value of $\lambda = 0.15$. Manning's roughness coefficients were varied by ± 30% with respect to the reference configuration. In addition, an alternative runoff generation scheme was tested by activating the Green-Ampt infiltration module within the 2D model, allowing infiltration losses to be computed internally rather than prescribed via net rainfall. Green-Ampt parameters ([50]) were selected based on the dominant loam soil texture within the basin, according to the *Topsoil physical properties for Europe* maps based on LUCAS topsoil data ([51]), using literature-based reference ranges (Table A3, cfr. [52–54]).

Table A3
Literature ranges and values assumed in this study for the Green-Ampt method parameters.

Parameter (units)	Literature range	Values assumed in this study
Ψ: Suction (mm)	[88−200]	200
Ks: Saturated conductivity (mm/h)	[5-12]	12
Δθ: difference between saturated and initial water content (fraction)	[0.1 - 0.4]	0.3

Figure A3 summarizes the hydraulic response simulated at the selected cross-section 1–1′. The location of the cross-section relative to the wastewater treatment plant and surrounding infrastructure is shown in Fig. A3a, while the corresponding digital terrain profile is reported in Fig. A3b.

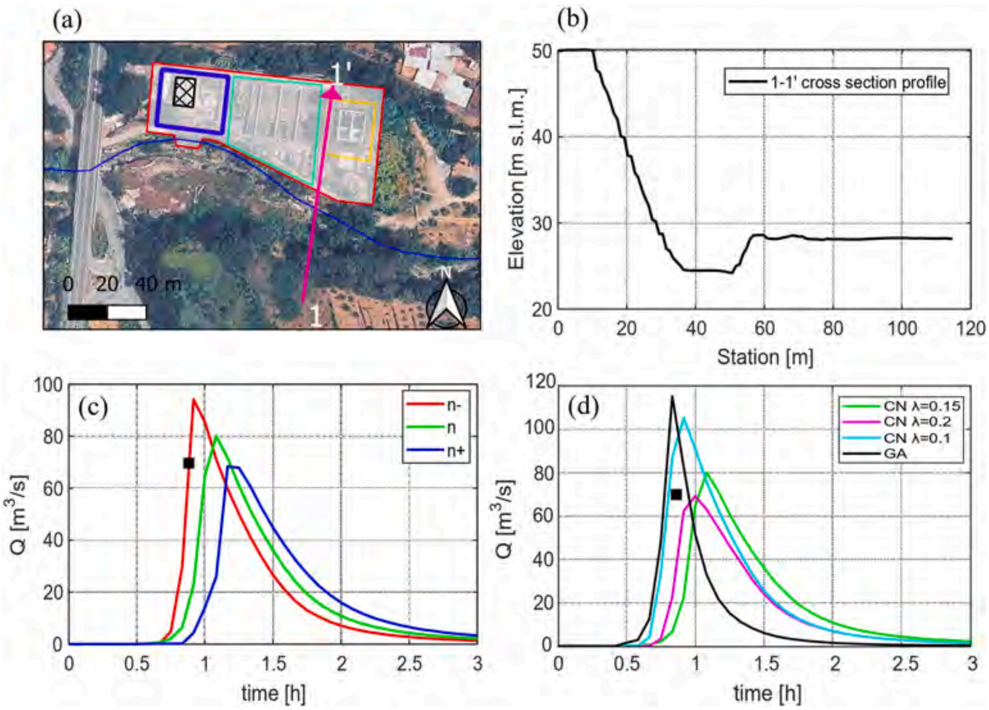

Fig. A3. Location of the computational cross-section (a) and corresponding digital terrain profile (b). Simulated discharge hydrographs $Q(t)$ obtained by varying Manning's roughness distributions using the SCS–CN method for rainfall losses (c). Comparison of discharge hydrographs computed with the reference Manning's roughness distribution using the SCS–CN, for three initial abstraction coefficients and Green–Ampt infiltration methods (d). Output time interval is 5 minutes. The black square indicates the estimate obtained using the rational method for a time of concentration of 0.86 h.

The sensitivity of the simulated flood hydrographs to channel roughness is illustrated in Fig. A3c. Discharge hydrographs were obtained by varying Manning's roughness coefficient by ±30% around the reference spatial distribution (n), while rainfall losses were computed using the SCS–CN method. These variations result in peak discharge changes of approximately −20% for the increased-roughness scenario (n−) and +20% for the reduced-roughness scenario (n+). Figure A3d compares discharge hydrographs obtained using the reference roughness distribution under different initial abstraction coefficients for the SCS–CN approach and Green-Ampt method as an alternative infiltration scheme.

The reference simulation combines spatially distributed Manning's roughness (*n*) with rainfall losses estimated via the SCS–CN method under AMC III conditions and an initial abstraction coefficient of 0.15. The resulting peak discharge ($80\ m^3\ s^{-1}$) is consistent with the preliminary estimate obtained from the rational method (peak discharge = $71.9\ m^3\ s^{-1}$, time of concentration = 0.86 h, estimated using the procedure described by Ref. [55].

Relative to the reference configuration, the Green–Ampt infiltration scheme produces a more impulsive hydrological response, with peak discharge approximately 40% higher, while variations in initial abstraction lead to peak discharge differences ranging from −13 to +33%. Across all simulations, the catchment exhibits a rapid hydrological response, characterised by short rising limbs and sharp discharge peaks. Overall, this variability is not expected to materially affect the outcomes of the cascading hazard assessment framework: even under an intermediate scenario, the flood hydrograph remains sufficient to reach the WWTP in the presence of an in-channel sediment deposit, and analogous results are expected across all alternative parameterisations and infiltration schemes.

Data availability

Data will be made available on request.

References

[1] L. Cremonini, P. Randi, M. Fazzini, M. Nardino, F. Rossi, T. Georgiadis, Causes and impacts of flood events in Emilia-Romagna (Italy) in May 2023, Land 13 (2024) 1800, https://doi.org/10.3390/land13111800.
[2] V. Gallina, S. Torresan, A. Critto, A. Sperotto, T. Glade, A. Marcomini, A review of multi-risk methodologies for natural hazards: consequences and challenges for a climate change impact assessment, J. Environ. Manag. 168 (2016) 123–132, https://doi.org/10.1016/j.jenvman.2015.11.011.
[3] A. Tilloy, B.D. Malamud, H. Winter, A. Joly-Laugel, A review of quantification methodologies for multi-hazard interrelationships, Earth Sci. Rev. 196 (2019) 102881, https://doi.org/10.1016/j.earscirev.2019.102881.
[4] S. De Angeli, B.D. Malamud, L. Rossi, F.E. Taylor, E. Trasforini, R. Rudari, A multi-hazard framework for spatial-temporal impact analysis, Int. J. Disaster Risk Reduct. 73 (2022) 192829, https://doi.org/10.1016/j.ijdrr.2022.102829.
[5] K. Barquet, M. Englund, K. Inga, K. André, L. Segnestam, Conceptualising multiple hazards and cascading effects on critical infrastructures, Disasters 48 (1) (2023) e12591, https://doi.org/10.1111/disa.12591.
[6] M. Nones, G. Pescaroli, Implications of cascading effects for the EU Floods Directive, Int. J. River Basin Manag. 14 (2) (2016) 195–204, https://doi.org/10.1080/15715124.2016.1149074.
[7] T.-E. Antofie, S. Luoni, A. Tilloy, A. Sibilia, S. Salari, G. Eklund, D. Rodomonti, C. Bountzouklis, C. Corbane, Spatial identification of regions exposed to multi-hazards at the Pan-European level, Nat. Hazards Earth Syst. Sci. 25 (2025) 287–304, https://doi.org/10.5194/nhess-25-287-2025.
[8] G. Forzieri, L. Feyen, S. Russo, et al., Multi-hazard assessment in Europe under climate change, Clim. Change 137 (2016) 105–119, https://doi.org/10.1007/s10584-016-1661-x.
[9] X. Ming, Q. Liang, R. Dawson, X. Xia, J. Hou, A quantitative multi-hazard risk assessment framework for compound flooding considering hazard inter-dependencies and interactions, J. Hydrol. 607 (2022) 127477, https://doi.org/10.1016/j.jhydrol.2022.127477.
[10] H.D. Skilodimou, G.D. Bathrellos, K. Chousianitis, et al., Multi-hazard assessment modeling via multi-criteria analysis and GIS: a case study, Environ. Earth Sci. 78 (2019) 47, https://doi.org/10.1007/s12665-018-8003-4.
[11] S. Yousefi, H.R. Pourghasemi, S.N. Emami, et al., A machine learning framework for multi-hazards modeling and mapping in a mountainous area, Sci. Rep. 10 (2020) 12144, https://doi.org/10.1038/s41598-020-69233-2.
[12] A.M. Youssef, A.M. Mahdi, H.R. Pourghasemi, Landslides and flood multi-hazard assessment using machine learning techniques, Bull. Eng. Geol. Environ. 81 (2022) 370, https://doi.org/10.1007/s10064-022-02874-x.
[13] H. Löfroth, G. Göransson, J. Hedfors, et al., Developing a methodology for characterizing cascading natural hazards associated with landslide risk in Sweden, Nat. Hazards 121 (2025) 22915–22933, https://doi.org/10.1007/s11069-025-07706-1.
[14] M. Castiglione, M. Capodici, S.F. Corsino, A. Cosenza, M. Torregrossa, Multi-natural hazard mapping for critical infrastructures in complex territorial contexts: proposal of a novel methodological approach, J. Environ. Manag. 400 (2026) 128767, https://doi.org/10.1016/j.jenvman.2026.128767.
[15] M.P. Boni, A. Faiella, V. Gazzola, F. Pergalani, A multi-hazard and multi-risk assessment methodological approach to support Civil Protection planning in wide areas, Int. J. Disaster Risk Reduct. 119 (2025) 105343, https://doi.org/10.1016/j.ijdrr.2025.105343.
[16] B. Tansel, Multi-hazard vulnerability and impact intensification: interactive hazards and impact compounding in coastal areas, Int. J. Disaster Risk Reduct. 131 (2025) 105883, https://doi.org/10.1016/j.ijdrr.2025.105883.
[17] J. Kwon, S. Yu, M. Malecha, P. Berke, Multi-Hazard assessment methods for planning: a review and potential future directions, Sustain. Cities Soc. 137 (2026) 107136, https://doi.org/10.1016/j.scs.2026.107136.
[18] H.T. Nguyen, T. Wiatr, T.M. Fernández-Steeger, et al., Landslide hazard and cascading effects following the extreme rainfall event on Madeira Island (February 2010), Nat. Hazards 65 (2013) 635–652, https://doi.org/10.1007/s11069-012-0387-y.
[19] C. Song, C. Yu, Z. Li, et al., Triggering and recovery of earthquake accelerated landslides in Central Italy revealed by satellite radar observations, Nat. Commun. 13 (2022) 7278, https://doi.org/10.1038/s41467-022-35035-5.
[20] B. Mazzorana, F. Comiti, C. Scherer, S. Fuchs, Developing consistent scenarios to assess flood hazards in mountain streams, J. Environ. Manag. 94 (2012) 112–124, https://doi.org/10.1016/j.jenvman.2011.06.030.
[21] F.K. Rengers, L.A. McGuire, J.W. Kean, D.M. Staley, D.E.J. Hobley, Model simulations of flood and debris flow timing in steep catchments after wildfire, Water Resour. Res. 52 (8) (2016) 6041–6061, https://doi.org/10.1002/2015WR018176.
[22] G. Esposito, A. Parodi, M. Lagasio, R. Masi, G. Nanni, F. Russo, S. Alfano, G. Giannatiempo, Characterizing consecutive flooding events after the 2017 Mt. Salto wildfires (Southern Italy): Hazard and emergency management implications, Water 11 (12) (2019) 2663, https://doi.org/10.3390/w11122663.
[23] C. Arrighi, M. Masi, R. Iannelli, Flood risk assessment of environmental pollution hotspots, Environ. Model. Software 100 (2018) 1–10, https://doi.org/10.1016/j.envsoft.2017.11.014.
[24] R. Nazari, H. Vasiliadis, M. Karimi, M.G.R. Fahad, S. Simon, T. Zhang, Q. Sun, R. Peters, Hydrodynamic Study of the impact of extreme flooding events on wastewater treatment plants considering total water level, Nat. Hazards Rev. 23 (1) (2021), https://doi.org/10.1061/(ASCE)NH.1527-6996.0000531.

[25] F. Aziz, X. Wang, M. Qasim Mahmood, R. Guild, Wastewater flooding risk assessment for coastal communities: compound impacts of climate change and population growth, J. Hydrol. 645 (2024) 132136, https://doi.org/10.1016/j.jhydrol.2024.132136.

[26] S. Bolan, L.P. Padhye, T. Jasemizad, M. Govarthanan, N. Karmegam, H. Wijesekara, D. Amarasiri, D. Hou, P. Zhou, B.K. Biswal, R. Balasubramanian, H. Wang, K. H.M. Siddique, J. Rinklebe, M.B. Kirkham, N. Bolan, Impacts of climate change on the fate of contaminants through extreme weather events, Sci. Total Environ. 909 (2024) 168388, https://doi.org/10.1016/j.scitotenv.2023.168388.

[27] J. Petrucci, J. Jalbert, S. Dorner, N. McQuaid, F. Bichai, Strategic prioritization of sewersheds to mitigate combined sewer overflows under climate change, Environ. Chall. 18 (2025) 101088, https://doi.org/10.1016/j.envc.2025.101088.

[28] C.J. White, M.S.G. Adnan, M. Arosio, S. Buller, Y. Cha, R. Ciurean, J.M. Crummy, M. Duncan, J. Gill, C. Kennedy, E. Nobile, L. Smale, P.J. Ward, Review article: towards multi-hazard and multi-risk indicators – a review and recommendations for development and implementation, Nat. Hazards Earth Syst. Sci. 25 (2025) 4263–4281, https://doi.org/10.5194/nhess-25-4263-2025.

[29] P. Claps, G. Evangelista, D. Ganora, P. Mazzoglio, I. Monforte, FOCA: a new quality-controlled database of floods and catchment descriptors in Italy, Earth Syst. Sci. Data 16 (2024) 1503–1522, https://doi.org/10.5194/essd-16-1503-2024.

[30] C.J. Keifer, H.H. Chu, Synthetic storm pattern for drainage design, J. Hydraul. Div. 83 (4) (1957) 1332, https://doi.org/10.1061/jyceaj.0000104.

[31] A. Viglione, G. Blöschl, On the role of storm duration in the mapping of rainfall to flood return periods, Hydrol. Earth Syst. Sci. 13 (2009) 205–216, https://doi.org/10.5194/hess-13-205-2009.

[32] A. Viglione, R. Merz, G. Blöschl, On the role of the runoff coefficient in the mapping of rainfall to flood return periods, Hydrol. Earth Syst. Sci. 13 (5) (2009) 577–593, https://doi.org/10.5194/hess-13-577-2009.

[33] G. Evangelista, P. Bogoni, D. Ganora, P. Claps, Quantifying representative runoff coefficients for small basins: a practical recipe for data-limited conditions, Hydrol. Sci. J. (2026), https://doi.org/10.1080/02626667.2026.2665734.

[34] B. Bout, V.G. Jetten, The validity of flow approximations when simulating catchment-integrated flash floods, J. Hydrol. 556 (2018) 674–688, https://doi.org/10.1016/j.jhydrol.2017.11.033.

[35] F. Macchione, M. Lombardo, Roughness-Based method for simulating hydraulic consequences of both woody debris clogging and breakage at bridges in basin-scale flood modeling, Water Resour. Res. 57 (12) (2021) e2021WR030485, https://doi.org/10.1029/2021WR030485.

[36] P. Costabile, L. Cea, G. Barbaro, C. Costanzo, M. Llena, D. Vericat, Evaluation of 2D hydrodynamic-based rainfall/runoff modelling for soil erosion assessment at a seasonal scale, J. Hydrol. 632 (2024) 130778, https://doi.org/10.1016/j.jhydrol.2024.130778.

[37] L. Cea, M. Álvarez, J. Puertas, Using integrated hydrological-hydraulic modelling and global data sources to analyse the February 2023 floods in the Umbeluzi Catchment (Mozambique), Nat. Hazards Earth Syst. Sci. 24 (1) (2024) 225–243, https://doi.org/10.5194/nhess-24-225-2024.

[38] F. Wang, C. Ouyang, H. An, X. Chen, S. Zhou, Q. Xu, A flash flood Numerical modeling and forecasting tool in mountainous small catchments based on a 2-D hydrodynamic model, Earth Space Sci. 12 (7) (2025) e2024EA004076, https://doi.org/10.1029/2024EA004076.

[39] P. Costabile, M. Lombardo, C. Costanzo, I. Tsoukalas, V. Bellos, A stochastic rain-on-grid framework for handling spatio-temporal rainfall uncertainty in impact-based flood nowcasting, Int. J. Disaster Risk Reduct. 134 (2026) 105998, https://doi.org/10.1016/j.ijdrr.2026.105998.

[40] P. Costabile, A. Maranzoni, Enhancing 2D hydrodynamic-based flash flood simulations in mountain catchments: analytical insights from a novel steep-slope shallow water framework, Water Resour. Res. 62 (5) (2026) e2025WR041653, https://doi.org/10.1029/2025WR041653.

[41] B.M.T. Wbm, *TUFLOW User Manual – Build 2025.1.0*. BMT Commercial Australia, 2018.

[42] F. Guzzetti, F. Ardizzone, M. Cardinali, M. Rossi, D. Valigi, Landslide volumes and landslide mobilization rates in Umbria, central Italy, Earth Planet Sci. Lett. 279 (3–4) (2009) 222–229, https://doi.org/10.1016/j.epsl.2009.01.005.

[43] G.M. Saulnier, K. Beven, C. Obled, Including spatially variable effective soil depths in TOPMODEL, J. Hydrol. 202 (1997) 158–172, https://doi.org/10.1016/S0022-1694(97)00059-0.

[44] L. Schilirò, A. Cevasco, C. Esposito, G.S. Mugnozza, Shallow landslide initiation on terraced slopes: inferences from a physically based approach, Geomat. Nat. Hazards Risk 9 (1) (2018) 295–324, https://doi.org/10.1080/19475705.2018.1430066.

[45] Y. Xing, D. Shao, Q. Liang, H. Chen, X. Ma, I. Ullah, Investigation of the drainage loss effects with a street view based drainage calculation method in hydrodynamic modelling of pluvial floods in urbanized area, J. Hydrol. 605 (2022) 127365, https://doi.org/10.1016/j.jhydrol.2021.127365.

[46] Y. Wang, A.S. Chen, G. Fu, S. Djordjević, C. Zhang, D.A. Savić, An integrated framework for high-resolution urban flood modelling considering multiple information sources and urban features, Environ. Model. Software 107 (2018) 85–95, https://doi.org/10.1016/j.envsoft.2018.06.010.

[47] C. Montalvo, J.D. Reyes-Silva, E. Sañudo, L. Cea, J. Puertas, Urban pluvial flood modelling in the absence of sewer drainage network data: a physics-based approach, J. Hydrol. 634 (2024) 131043, https://doi.org/10.1016/j.jhydrol.2024.131043.

[48] H. Apel, J. Benisch, B. Helm, S. Vorogushyn, B. Merz, Fast urban inundation simulation with RIM2D for flood risk assessment and forecasting, Front. Water 6 (2024) 1310182, https://doi.org/10.3389/frwa.2024.1310182.

[49] K. Guo, M. Guan, H. Yan, X. Xia, A spatially distributed hydrodynamic model framework for urban flood hydrological and hydraulic processes involving drainage flow quantification, J. Hydrol. 625 (2023) 130135, https://doi.org/10.1016/j.jhydrol.2023.130135.

[50] W.H. Green, G.A. Ampt, Studies on soil physics, J. Agric. Sci. 4 (1) (1911) 1–24.

[51] C. Ballabio, P. Panagos, L. Montanarella, Mapping topsoil physical properties at European scale using the LUCAS database, Geoderma 261 (2016) 110–123, https://doi.org/10.1016/j.geoderma.2015.07.006.

[52] W.J. Rawls, D.L. Brakensiek, N. Miller, Green-Ampt infiltration parameters from soils data, J. Hydraul. Eng. 109 (1) (1983) 62–70.

[53] S. Gupta, A. Papritz, P. Lehmann, T. Hengl, S. Bonetti, D. Or, Global Soil Hydraulic Properties dataset based on legacy site observations and robust parameterization, Sci. Data 9 (1) (2022) 444, https://doi.org/10.1038/s41597-022-01481-5.

[54] Innovyze Manual. https://help2.innovyze.com/infoworksicm/Content/HTML/ICM_ILCM/Green-Ampt_Model.htm.

[55] G. Evangelista, R. Woods, P. Claps, Towards robust operational estimation of the time of concentration in ungauged basins, in: Proceedings of the XXXIX Convegno Nazionale di Idraulica e Costruzioni Idrauliche, September 15-18, 2024. Parma (Italy).